4354 *Biochemistry* **2009,** *48,* 4354–4370
DOI:10.1021/bi802361k

BIOCHEMISTRY
including biophysical chemistry & molecular biology
Article

Aβ_{40}, either Soluble or Aggregated, Is a Remarkably Potent Antioxidant in Cell-Free Oxidative Systems

Rozena Baruch-Suchodolsky and Bilha Fischer*

Department of Chemistry, Gonda-Goldschmied Medical Research Center, Bar-Ilan University, Ramat-Gan 52900, Israel

Received December 28, 2008. Revised Manuscript Received March 25, 2009

ABSTRACT: The brains of individuals diagnosed with Alzheimer's disease (AD) are characterized by amyloid plaques, of which the major component is Aβ peptide. Excessive Cu and Fe ions binding to Aβ were suggested to have a deleterious effect on promoting both the aggregation of Aβ and the generation of reactive oxygen species (ROS). Other studies suggested that Aβ plays a protective role by acting as an antioxidant at nanomolar concentrations. The apparent confusion regarding the antioxidant and prooxidant properties of Aβ_{40} encouraged us to explore the modulatory role of Aβ_{40} at the molecular level under oxidative stress conditions. Here, we focused on Aβ_{40} in the simplest oxidative system, namely, Cu(I)/Cu(II)/Fe(II)-H_2O_2. Using ESR, we monitored the production of OH radicals in the above-mentioned systems in the presence of Aβ_{40}. We found that Aβ_{40}, either in its soluble or in its aggregated form, functioned as a remarkably potent antioxidant in Cu(I)/Fe(II)-catalyzed radical-producing systems and slightly less potently in the presence of Cu(II) with IC_{50} values of 13−62 μM. Aβ_{40} proved to be 3.8−6.5 and 15−42 times more potent than the soluble Aβ_{28} and the potent antioxidant Trolox, respectively, in the Cu(I)/Fe(II)-H_2O_2 systems. Time-dependent enhancement of ROS production by Aβ_{40} occurs only at low concentrations of aggregated Aβ_{40} and in the presence of Cu(II). On the basis of the extremely low IC_{50} values of Aβ_{40} and the extensive oxidative damage caused to Aβ_{40} in Cu(I)/Fe(II)-H_2O_2 systems, we propose that radical scavenging is the major mechanism of antioxidant activity of Aβ_{40} in addition to metal ion chelation. In summary, Aβ_{40}, either soluble or aggregated, at either nanomolar or micromolar concentrations is a highly potent antioxidant in cell-free oxidative systems, acting mainly as a radical scavenger. Therefore, we propose that it is not the Aβ_{40}−Cu(I)/Fe(II) complex per se that is responsible for the oxidative damage in AD.

The brains of individuals diagnosed with Alzheimer's disease (AD)[1] are characterized by amyloid plaques, of which the major component is amyloid β (Aβ) peptide, a 39−43-amino acid residue peptide (*1*,*2*). Amyloid deposition was suggested to be a critical step in the neurodegenerative process associated with AD (*3*). In addition, AD brain tissue is characterized by unusually high concentrations of zinc, copper, and iron ions (*4*). Thus, Cu(II) and Fe(III) have been found at concentrations of ~0.4 and 1 mM, respectively, in amyloid plaques (*5*).

Excessive Cu(II) binding, and to a lesser extent Fe(III) binding (*6*), to Aβ was suggested to have a deleterious effect on promoting the aggregation and redox activities of the Aβ proteins (*7*). Aβ was shown to be neurotoxic in vitro when incubated with Cu(II) or Fe(III) (*8*,*9*). Several studies showed that the structural transition (from random coil to β-sheet) from monomeric to fibrillar peptide was required for toxicity (*10*,*11*). Other studies indicated that the presence of transition metals may be required for both Aβ fibrillization and the initiation of reactive oxygen species (ROS) generation (*12*).

ROS, such as OH radicals, were proposed to trigger neurotoxicity in AD (*13*,*14*). OH radicals may be formed by the Fe(II) or Cu(I) ion-catalyzed H_2O_2 decomposition (Fenton reaction): Fe(II) + H_2O_2 → Fe(III) + $^{\bullet}$OH + OH^- (*15*−*17*).

The decomposition of H_2O_2 to produce $^{\bullet}$OH is also induced by Cu(II) or Fe(III) ions (Haber−Weiss-like mechanism) (*18*−*20*), shown here for Cu(II) ion (eqs 1−4) (*21*,*22*):

$$Cu(II) + H_2O_2 \rightarrow Cu(I)^{\bullet}O_2H + H^+ \quad (1)$$

$$Cu(I)^{\bullet}O_2H + H_2O_2 \rightarrow Cu(I) + O_2 + {}^{\bullet}OH + H_2O \quad (2)$$

$$Cu(I) + H_2O_2 \rightarrow Cu(II) + {}^{\bullet}OH + OH^- \quad (3)$$

$$3H_2O_2 \rightarrow O_2 + 2{}^{\bullet}OH + 2H_2O \quad (4)$$

*To whom correspondence should be addressed. Telephone: 972-3-5318303. Fax: 972-3-6354907. E-mail: bfischer@mail.biu.ac.il.

[1]Abbreviations: AD, Alzheimer's disease; BCA, bicinchoninic acid; CR, Congo red; DMPO, 5,5′-dimethyl-1-pyrroline-*N*-oxide; ESR, electron spin resonance; HFIP, hexafluoroisopropanol; ICP, inductively coupled plasma; PAGE, polyacrylamide gel electrophoresis; pI, isoelectric point; ROS, reactive oxygen species; SDS, sodium dodecyl sulfate; TEM, transmission electron microscopy; TFA, trifluoroacetic acid; Tris, tris(hydroxymethyl)aminomethane.

Published on Web 3/25/2009

The reduction of Cu(II) and Fe(III) ions in the Aβ complex, to form the reactive Cu(I) and Fe(II) ions, respectively, was proposed to occur by either Met35 in A$\beta_{40/42}$ (*23*,*24*) or cellular reductants (*25*). This reduction of the Aβ-coordinated metal ions (*26*) allows the Aβ−metal ion complex to produce in vitro H_2O_2 from O_2 (*24*), and subsequently OH radicals from H_2O_2 decomposition (*24*). Thus, the Aβ−metal ion complex acts as an *oxidant*, as shown for cell cultures in the presence of Cu(II) (*8*,*27*).

On the other hand, significant evidence indicates the contrary, that the formation of diffuse amyloid plaques may be considered as a compensatory response that reduces oxidative stress (*28*,*29*) and that the accumulation of Aβ in the AD brain may be related to an increased oxidative challenge (*30*). This finding suggests an *antioxidant* function of Aβ.

Atwood et al. reviewed the evidence pointing at either the antioxidant or oxidant function of A$\beta_{40/42}$ and proposed the following solution to the apparent contradiction concerning the oxidant or antioxidant function of Aβ (*31*):

The increased generation of Aβ following oxidative stress indicates a response to preserve normal cellular function by reducing oxidative insults. However, at some threshold level of ROS generation, efficient removal of Aβ−metal complexes would be overtaken by their disproportionably high level of generation, resulting in the uncontrollable growth of plaques. This growth consequently may overwhelm antioxidant defense systems incapable of handling the accumulation of H_2O_2. Thus, Aβ−Cu deposits are predicted to be neurotoxic if H_2O_2 is produced above the threshold level of removal. This activity results in a vicious cycle of increased Aβ generation and ROS production leading to neurotoxicity (*32*).

Therefore, to accelerate oxidation, Aβ must be present at concentrations that greatly exceed those normally measured in biological fluids or tissues (i.e., micromolar vs nanomolar) (*33*,*34*). This finding has been reported for cerebrospinal fluid, where Aβ acts as an antioxidant at concentrations of 0.1−1.0 nM, while at higher Aβ concentrations, its antioxidant action is abolished (*35*).

The apparent confusion regarding the antioxidant and pro-oxidant properties of A$\beta_{40/42}$ emphasizes the urgent need to systematically explore the modulatory role of A$\beta_{40/42}$ under oxidative stress conditions.

Recently, we studied, using ESR, the modulation of Cu/Fe-induced H_2O_2 decomposition by Aβ_{1-28} (Aβ_{28}), a soluble model of A$\beta_{40/42}$ (*36*). We found that the addition of H_2O_2 to 0.6 nM to 360 μM Aβ_{28} solutions containing 100 μM Cu(II), Cu(I), or Fe(II) at pH 6.6 resulted in a concentration-dependent inhibition of OH radical formation with IC_{50} values of 61, 59, and 84 μM, respectively. Furthermore, Aβ_{28} reduced 90% of $^{\bullet}$OH production in the Cu(I)-H_2O_2 system in 5 min. Unlike soluble Aβ_{28}, the Aβ_{28}−Cu(I) aggregate exhibited poor antioxidant activity. On the basis of the analysis of the time-dependent percentage of oxidized Aβ_{28} [formed in the Cu(I)/Fe(II)-H_2O_2 systems], we proposed that the mechanism of antioxidant activity of soluble Aβ_{28} is two-fold. The primary (rapid) mechanism involves metal ion-chelation, whereas the secondary (slow) mechanism involves •OH scavenging and the subsequent oxidation of Cu(Fe)-coordinating ligands (His6, His13, His14, and Tyr10).

Our findings, indicating the potent antioxidant activity of soluble Aβ_{28} in cell-free systems, encouraged us to study the modulatory properties of the endogenous peptide, Aβ_{40}, under oxidative conditions in cell-free systems.

To directly explore the modulation of OH radicals' production from H_2O_2 by Aβ, we focused on removing the immense complexity and numerous cross interactions occurring in cells and focusing on the "naked" Aβ in the simplest oxidative system possible, namely, Cu(I)/Cu(II)/Fe(II) in the presence of H_2O_2. Thus, we first targeted the evaluation of the modulatory capacity of soluble Aβ_{40} in the systems described above. Moreover, we wanted to learn if aggregation changes the modulatory function of soluble Aβ_{40}. In addition, we aimed to decipher the mechanism(s) by which Aβ_{40} modulates OH radicals' production.

Here, we provide evidence of the unexpectedly high antioxidant activity of Aβ_{40} in oxidizing systems [Cu(I)/Cu(II)/Fe(II)-H_2O_2] and its dependence on the Aβ concentration, Aβ's solubility, metal ion type, and time. In addition, on the basis of time-dependent amino acid analysis of Aβ in these oxidizing systems, we proposed a mechanism to explain the Aβ_{40} antioxidant function as compared to the function of Aβ_{28} and a standard antioxidant.

EXPERIMENTAL PROCEDURES

Materials. $FeSO_4 \cdot 7H_2O$ was purchased from J. T. Baker Inc. (Phillipsburg, NJ). A 10 g/L copper nitrate standard solution was purchased from Merck. Tetrakis (acetonitrile)copper(I) hexafluorophosphate and bicinchoninic acid disodium salt (BCA) were purchased from Aldrich Chemicals Co. Congo red, 5,5′-dimethyl-1-pyrroline-*N*-oxide (DMPO), tris(hydroxymethyl)aminomethane (ultra pure), amyloid β-protein fragment 1−40, and amyloid β-protein fragment 1−28 were purchased from Sigma Chemical Co. Hydrogen peroxide (30% solution) was obtained from Frutarom Ltd. (Haifa, Israel). All reagents for Native PAGE were electrophoresis grade and were purchased from Bio-Rad Laboratories. We purified the $Cu(CH_3CN)_4PF_6$ before it was used by dissolving it in acetonitrile (HPLC grade) and twice filtered the insoluble Cu(II) salt by a syringe nylon 0.45 μm filter. The filtrate was deaerated with an argon stream. $FeSO_4 \cdot 7H_2O$ was recrystallized twice from water and ethanol before use. The concentration of the Cu(I) salt was determined by UV spectroscopy with the addition of the specific Cu(I) indicator, BCA (ε_{562} = 7700 M^{-1}) (*37*). Aqueous solutions were freshly prepared with HPLC grade water (Bio Laboratory Ltd.). The spin trap DMPO was purified by mixing a spatula of activated charcoal with 1 mL of an ~0.4 M DMPO solution, for ~30 min in the dark. The solution was then filtered, and the exact concentration of DMPO was determined by UV spectroscopy (ε_{228} = 8000 M^{-1}) (*38*). The DMPO solution was deaereted with an argon stream and stored at −18 °C for no more than 2 weeks after purification. All other commercial products were used without any purification. Crude Aβ_{28} was purified by HPLC over a Chromolith performance RP-18E column (100 mm × 4.6 mm), applying a linear gradient of 13 to 45% B over

30 min [A is 0.1% trifluoroacetic acid (TFA) in H_2O, and B is a 3:1 acetonitrile/A mixture]. The solution of the purified peptide was filtered over a PVDF 0.45 μm filter. The peptide purity was determined by ^{1}H NMR using a pure reference. The pure freeze-dried Aβ_{28} was dissolved in water (HPLC grade) to give 0.6−1.2 mM stock solutions, and the stock solutions were stored at −20 °C. Due to the limited solubility of Aβ_{28}, it was impossible to obtain more concentrated solutions. Soluble Aβ_{40} solutions were prepared according to the "NaOH method" (*39*). Specifically, Aβ_{40} (TFA salt, 1 mg) was dissolved in 2 mM NaOH (1 mL), and additional 0.1 M NaOH (~30 μL) was required for complete dissolution of the protein (final pH of ~11). The Aβ_{40} solution was then sonicated for 15 min, until the solution became clear. The solution was divided into aliquots and freeze-dried. The resulting solid Aβ_{40} was stored at −20 °C. All solutions were prepared from ddH_2O.

General. OH radicals produced from H_2O_2 by Fe(II) or Cu(I/II) ion catalysis were detected by ESR spectroscopy using a Bruker ER 100d X-band spectrophotometer. ESR settings were as follows: microwave frequency, 9.76 GHz; modulation frequency, 100 kHz; microwave power, 6.35 mW; modulation amplitude, 1.2 G; time constant, 655.36 ms; sweep time, 83.89 s; and receiver gain, 2×10^5 for Fe(II)-H_2O_2 and Cu(I)-H_2O_2 systems or 2×10^6 for the Cu(II)-H_2O_2 system. After being acquired, the spectra were processed with Bruker WIN-EPR version 2.11 for integration of the signals. The integration of the second signal of the DMPO-OH spin adduct quartet is expressed as a percentage of the control [control solutions contained only Cu(I/II)- or Fe(II)-H_2O_2 solutions]. ESR measurements were repeated two to five times on different days. Absorption data were measured on a Shimadzu UV−vis recording spectrophotometer (UV-2401PC).

Characterization of Soluble Aβ_{40}−Cu(I)/Cu(II)/Fe(II) Complexes. (1) Preparation of Soluble Aβ_{40} Stock Solutions. A 1 mM soluble amyloid-β 1−40 stock solution was prepared by dissolving the above 1 mg of freeze-dried Aβ_{40} in 10 mM Tris buffer (pH 7.4, 230 μL). To minimize isoelectric precipitation of Aβ_{40} (which occurs between pH 4 and 7) (*40*), the pH of the protein solution should not drop below pH 7 [Aβ_{40} aggregates at pH 5−7, which is around the pI point (*41*)] (*42*). Dissolution of Aβ_{40} NaOH salt in Tris buffer (pH 7.4) resulted in a slightly basic solution, the pH of which was adjusted by 0.1 M HCl back to 7.4. All Aβ_{40} stock solutions were filtered from nonsoluble components over a PVDF 0.22 μm filter (*43*).

(2) Preparation of the Aβ_{40}−Cu(I) Complex and Determination of the Cu(I) Concentration in the Soluble Aβ_{40}−Cu(I) Complex. (i) Preparation of UV Samples. **Control 1**, containing BCA and Cu(I), was prepared by adding 2 mM Cu$(CH_3CN)_4PF_6$ in acetonitrile (10 μL) to a 0.05 M BCA (5 μL) stock solution, followed by the addition of 1 mM Tris buffer (pH 7.4) to a final sample volume of 1 mL. **Control 2**, containing BCA and Aβ_{40}, was prepared by adding a 0.7 mM soluble Aβ_{40} solution (20 μL) to a 0.05 M BCA (5 μL) stock solution, followed by the addition of 1 mM Tris buffer (pH 7.4) to a final sample volume of 1 mL. The **sample** was prepared by adding 2 mM Cu$(CH_3CN)_4PF_6$ in acetonitrile (10 μL) to a 0.7 mM soluble Aβ_{40} solution (20 μL). After the sample had been mixed for 30 s, 0.05 M BCA (5 μL) was added, followed by the addition of 1 mM Tris buffer (pH 7.4) to a final sample volume of 1 mL. The final component concentrations in a 1 mL sample were as follows: 150 μM BCA, 20 μM Cu(I), and 20 μM Aβ_{40}. The samples were measured 5 min and 3 days after preparation. The concentration of Cu(I) in the Aβ_{40}−Cu complex was quantified by UV spectroscopy using the Cu(I)-specific indicator, BCA. The typical absorbance of the Cu(I)−BCA complex at 560 nm (ε_{562} = 7700 M^{-1}) (*37*) was used to quantify the degree of oxidation, if any, of Cu(I) to Cu(II) in the presence of Aβ_{40} and atmospheric oxygen. The Cu(I) concentration determined with this method was 22−24 μM for both 5-min- or 3-day-old samples, consistent with the initial Cu(I) concentration. These results are within the UV spectrophotometer measurement error, indicating that Cu(I) is stable in its Aβ complex under ESR measurement conditions.

(3) Native Polyacrylamide Gel Electrophoresis (Native PAGE). (i) Sample Preparation. The gel samples, described below, were not denaturated by heating, and the sample buffer did not contain SDS or β-mercaptoethanol. All samples were prepared and stored at 0 °C until they were loaded. The sample buffer was prepared as follows. First, 0.5 M Tris buffer (pH 6.8, 1 mL) was diluted with H_2O (3.8 mL), and then bromophenol blue B-0149 (0.1 g) was added, followed by the addition of excess glycerol (1.2 mL). Excess glycerol increases the density of the light peptide Aβ_{40} and helps in loading it onto the gel. The gel samples were prepared by adding 2 mM Cu$(CH_3CN)_4PF_6$ in acetonitrile (2 μL) or 1 mM Cu$(NO_3)_2$ (4 μL) or 1 mM $FeSO_4$ (4 μL) to a 0.161 mM soluble Aβ_{40} solution (25 μL). After an incubation period of 30 s, sample buffer (3 μL) was added to Aβ_{40}−Cu or −Fe complex solutions. The final component concentrations in a total volume of 32 μL were 0.11 mM $FeSO_4$/Cu$(NO_3)_2$/Cu$(CH_3CN)_4PF_6$ and 0.126 mM Aβ_{40}. Four control samples were prepared. **Control 1** contained only soluble Aβ_{40}. The sample was prepared by adding a 0.161 mM soluble Aβ_{40} solution (25 μL) to a sample buffer (3 μL). **Control 2** contained aggregated Aβ_{40}−Cu(I) complex. Aβ_{40}−Cu(I) aggregates were prepared by adding 10 mM Cu$(CH_3CN)_4PF_6$ in acetonitrile (11 μL) to 1 mg/mL Aβ_{40} solutions (500 μL); after a short period of mixing, the pH was adjusted to 1 [5 M HCl (5 μL)]. The solution was then neutralized to pH 7.5 [1 M NaOH (2 μL)], and the sample was allowed to mature for 3 days at room temperature to form aggregates. The sample was prepared by adding an Aβ_{40}−Cu(I) aggregate solution (25 μL) to the sample buffer (3 μL). The final component concentrations in a total volume of 28 μL were 0.2 mM Cu$(CH_3CN)_4PF_6$ and 0.14 mM Aβ_{40}. **Control 3** contained soluble Aβ_{28}−Cu(I) complex. The sample was prepared by adding 2 mM Cu$(CH_3CN)_4PF_6$ in acetonitrile (1 μL) to a 0.6 mM soluble Aβ_{28} solution (25 μL). After an incubation period of 30 s, a sample buffer (3 μL) was added to the Aβ_{28}−Cu(I) complex solution. The final component concentrations in a total volume of 29 μL were 0.1 mM Cu$(CH_3CN)_4PF_6$ and 0.06 mM Aβ_{28}. **Control 4** contained aggregated Aβ_{28}−Cu(I) complex. Aβ_{28}−Cu(I) aggregates were prepared by adding 11 mM Cu$(CH_3CN)_4PF_6$ in acetonitrile (2.5 μL) to a

0.6 mM Aβ_{28} solution (25 μL). After the sample had been mixed for 10 s, the pH was adjusted to ~7.5 with NaOH [0.025 M NaOH (10 μL)]. Aggregates were allowed to mature for 1 month at room temperature. The sample was prepared by adding an Aβ_{28}−Cu(I) aggregate solution (25 μL) to a sample buffer (3 μL). The final component concentrations in a total volume of 28 μL were 0.2 mM Cu$(CH_3CN)_4PF_6$ and 0.36 mM Aβ_{28}.

(ii) Native PAGE Protocol. Nondenaturing (without SDS) 15% polyacrylamide Tris-HCl gels, in a Tris-glycine buffer system, were used for monitoring the Aβ_{40} species by native electrophoresis. Native PAGE was uploaded with samples (25 μL), and the gels were electrophoresed at 100 V for 1.5 h at 4 °C. After electrophoresis, the gels were washed with a fixing solution (7% acetic acid with 50% methanol) for 30 min. The gels were stained overnight with 0.25% Coomassie blue (R250) dye or Sypro ruby red dye. The gels were destained three to five times, for 30 min each time, with a destaining solution (7% acetic acid with 50% methanol). All procedures were performed at 4 °C, and Sypro ruby red dye was visualized by fluorescence upon irradiation at 300 nm.

Determination of Concentration- and Time-Dependent Oxidant and Antioxidant Activity of Soluble Aβ_{40}−Cu(I)/Cu(II)/Fe(II) Complexes by ESR Measurements. **Control samples** were prepared by adding 1 mM $Cu(NO_3)_2$ (10 μL), 1 mM $FeSO_4$ (10 μL), or 2 mM $Cu(CH_3CN)_4PF_6$ in acetonitrile (5 μL) to 1 mM Tris buffer (70, 70, or 75 μL, respectively, at pH 7.4). After the sample had been mixed for 2 s, 20 mM DMPO (10 μL) was added quickly followed by 0.1 M H_2O_2 (10 μL). Final component concentrations in a total volume of 100 μL were 0.1 mM $Cu(NO_3)_2$/$Cu(CH_3CN)_4PF_6$, 2 mM DMPO, and 10 mM H_2O_2. For **soluble Aβ_{40} samples**, a 0.7 mM soluble Aβ_{40} stock solution was prepared by dissolution of 1 mg of freeze-dried Aβ_{40} (Aβ_{40} after NaOH treatment) in 1 mM Tris buffer (pH 7.4, 230 μL). The pH of the Aβ_{40} solution was adjusted with 0.1 M HCl to a final pH of 7.4. Less concentrated stock solutions were prepared by dilution of a 1 mM soluble Aβ_{40} stock solution. Concentrations of the stock solutions were from 0.7×10^{-4} to 0.7 mM. All of the Aβ_{40} stock solutions were filtered from nonsoluble components over a PVDF 0.22 μm filter. Two millimolar $Cu(CH_3CN)_4PF_6$ in acetonitrile (5 μL), 1 mM $Cu(NO_3)_2$ (10 μL), or 1 mM $FeSO_4$ (10 μL) was added to 0.7×10^{-4} to 0.7 mM soluble Aβ_{40} stock aqueous solutions (1−50 μL). After an incubation period of 30 s, 1 mM Tris buffer, pH 7.4 (20−75 μL) was added to Aβ_{40}−Cu/Fe ion solutions. After the sample had been mixed for 2 s, 20 mM DMPO (10 μL) was quickly added followed by 0.1 M H_2O_2 (10 μL). The final component concentrations in a total volume of 100 μL were 0.1 mM $FeSO_4$/$Cu(NO_3)_2$/$Cu(CH_3CN)_4PF_6$, 7 nM to 0.35 mM Aβ_{40}, 2 mM DMPO, and 10 mM H_2O_2. The final pH value of the Fe(II), Cu(I), and Cu(II) systems was 7.4 ± 0.01. The concentration-dependent oxidant or antioxidant activity of soluble Aβ_{40} was determined by ESR measurements 150 s [for Cu(I) and Fe(II)] and 20 min [for Cu(II)] after the addition of H_2O_2. All final solutions of Cu$(CH_3CN)_4PF_6$ contained 5% (v/v) acetonitrile. ESR measurements of the modulation of Cu(I)/Cu(II)/Fe(II)-induced H_2O_2 decomposition by soluble Aβ_{40} resulted in exponential decay graphs. IC_{50} values were calculated by fitting the data to a three-parameter exponential curve using SigmaPlot 9.0, with errors being taken as the deviation from the average value.

The time-dependent oxidant or antioxidant activity of soluble Aβ_{40}−Cu(I)/Cu(II)/Fe(II) samples was also determined by ESR measurements. The kinetics of the reaction was monitored for 1−2 h in 2−5 min intervals. Kinetic data are presented as the amount of DMPO-OH adduct, obtained by integration of the second peak of the DMPO-OH adduct quartet, versus time.

Preparation and Characterization of Aβ_{40}−Cu(I)/Cu(II) Aggregates. (1) Preparation. Aβ_{40}−Cu(I)/Cu(II) aggregates were prepared by either procedure A or B. In **procedure A**, 10 mM $Cu(CH_3CN)_4PF_6$ in acetonitrile (11 μL) was added to 1 mg/mL Aβ_{40} solutions (500 μL). After a short period of mixing, the pH was adjusted to 1 [5 M HCl (5 μL)] to induce aggregation. The pH of the solution was then adjusted to 7.5 [1 M NaOH (2 μL)]. A pH of 7.5 is not sufficiently basic to dissolve the aggregates. The final component concentrations were 0.23 mM $Cu(CH_3CN)_4PF_6$ and 0.161 mM Aβ_{40}. The aggregate sample was allowed to mature for 1 or 3 days at room temperature. In **procedure B**, an aggregated Aβ_{40} stock solution was prepared by adjusting the pH of a 1 mg/mL Aβ_{40} solution (500 μL) to 1 with 5 M HCl (5 μL) to induce aggregation and then neutralizing the solution to pH 7.5 with 1 M NaOH (2 μL). The aggregated Aβ_{40} stock solution was allowed to mature for 3 days at room temperature. Ten millimolar $Cu(CH_3CN)_4PF_6$ in acetonitrile (11 μL) was added to the aggregated Aβ_{40} stock solution, and the sample was analyzed within 1 h.

The Aβ_{40}−Cu(I) complex samples prepared according to procedure A were analyzed by UV using BCA as a Cu(I) indicator. The UV analysis indicated that those samples were totally oxidized after 3 days at room temperature under atmospheric oxygen. With procedure A, we obtained Aβ_{40}−Cu(II) complex aggregates. Moreover, Aβ_{40}−Cu aggregates, unlike soluble Aβ_{40}−Cu complexes, cannot stabilize Cu(I) ions for a long time.

(2) Characterization. (i) In the Congo red assay (*44*,*45*), a 2 mM Congo red stock solution was prepared in PBS (pH 7.4) and filtered three times on a cotton-plugged Pasteur pipet. Control samples, containing Congo red and Cu(I/II), were prepared by adding 2 mM Cu$(CH_3CN)_4PF_6$ in acetonitrile (15 μL) or 2 mM $Cu(NO_3)_2$ (10 μL) to a Congo red stock solution (10 μL), and PBS buffer was added to a final sample volume of 1 mL. An aggregate sample was prepared by adding a Congo red stock solution (10 μL) to an Aβ_{40}−Cu(II) fibril stock suspension (45 μL) [The fibril suspension was prepared by procedure A by mixing a 0.07 mM Aβ_{40} stock solution (30 μL) and 2 mM $Cu(CH_3CN)_4PF_6$ in acetonitrile (15 μL). This solution was acidified to pH 1 and then neutralized to pH 7.5 as described above. Aggregates were allowed to mature at room temperature for 1 or 3 days.] PBS buffer was added to a final sample volume of 1 mL. The aggregate sample prepared according to procedure B was made by adding 2 mM $Cu(CH_3CN)_4PF_6$ in acetonitrile (15 μL) to an Aβ_{40} fibril stock suspension (30 μL). Fibrils were prepared by acidifying an Aβ_{40} stock solution to pH 1 and then neutralized to pH 7.5. Aggregates

were allowed to mature at room temperature for 3 days, followed by the addition of a Congo red stock solution (10 μL). PBS buffer was added to a final sample volume of 1 mL, and the final component concentrations in a 1 mL sample were 20 μM Congo red, 30 μM Cu(I), and 21 μM Aβ_{40} fibrils. The typical absorbance of the Aβ fibril-bound dye was 490 nm. (ii) For TEM analysis, a TEM sample was prepared by applying 1 drop of the above Aβ_{40}−Cu(II) aggregate suspension on a grid, and water was vaporized at room temperature overnight. (iii) For ICP analysis, the sample was prepared by adding 2 mM $Cu(CH_3CN)_4PF_6$ in acetonitrile (5 μL) to a 0.7 mM soluble Aβ_{40} solution (10 μL). After the sample had been mixed for 10 s, the pH was adjusted to ~1 with HCl [5 M HCl (1 μL)]. The solution was then neutralized to pH 7.5 [0.5 M NaOH (10 μL)]. The final concentrations of components were 0.1 mM $Cu(CH_3CN)_4PF_6$ and 0.07 mM Aβ_{40}. The sample was allowed to mature for 3 days at room temperature, resulting in aggregates. The aggregates were then diluted with HPLC grade water to a final volume of 1 mL, followed by filtration of the aggregates over a 13 mm × 0.45 μm nylon Restek syringe filter. This filter absorbs Aβ [as we have previously demonstrated (*ref46*)]. The filtrate was diluted to a final volume of 5 mL and assayed by ICP. The filtrate contained practically no free Cu (0 mg/L) of the original 0.1 mM Cu in the ESR Aβ_{40}−Cu(II) sample. As a control, we filtered 0.1 mM Cu (II) through this filter and obtained a Cu(II) concentration of 0.1 mM by ICP measurement.

Concentration- and Time-Dependent Oxidant and Antioxidant Activity of Aggregated Aβ_{40}−Cu(I)/Cu(II) Complexes. **Control samples** were prepared by adding 1 mM $Cu(NO_3)_2$ (10 μL) or 2 mM $Cu(CH_3CN)_4PF_6$ in acetonitrile (5 μL) to 1 mM Tris buffer (70, 70, and 75 μL at pH 7.4). After the sample had been mixed for 2 s, 20 mM DMPO (10 μL) was added quickly followed by 0.1 M H_2O_2 (10 μL). The final component concentrations in a total volume of 100 μL were 0.1 mM $Cu(NO_3)_2$/$Cu(CH_3CN)_4PF_6$, 2 mM DMPO, and 10 mM H_2O_2. **Aggregated Aβ_{40}−Cu(I)/Cu(II) ESR samples** were prepared by either procedure A or B. For procedure A, 2 mM Cu $(CH_3CN)_4PF_6$ in acetonitrile (5 μL) was added to 0.07−0.7 mM soluble Aβ_{40} stock aqueous solutions (1−2 μL). After an incubation period of 30 s, 1 mM Tris buffer (pH 7.4, 73−74 μL) was added to Aβ_{40}−Cu(I) ion solutions (where necessary, the pH was adjusted to 7.4 with 0.1 M HCl). Samples were then incubated for 3 days at room temperature. After 3 days, 20 mM DMPO (10 μL) was added followed by 0.1 M H_2O_2 (10 μL). Final component concentrations in a total volume of 100 μL were 0.1 mM $Cu(CH_3CN)_4PF_6$, 1−20 μM Aβ_{40}, 2 mM DMPO, and 10 mM H_2O_2. The samples prepared according to method A were analyzed by UV using BCA as our Cu(I) indicator. The UV analysis indicated that those samples were oxidized after 3 days at room temperature under atmospheric oxygen; namely, we have obtained Aβ_{40}−Cu(II) complexes. With procedure B, an aggregated Aβ_{40} stock solution was prepared by adjusting the pH of the solution to 1 with 5 M HCl (5 μL) to induce aggregation and then neutralizing the solution to pH 7.5 with 1 M NaOH (2 μL). This Aβ_{40} stock suspension was allowed to mature for 3 days at room temperature. Two millimolar $Cu(CH_3CN)_4PF_6$ in acetonitrile (5 μL) was then added to a 0.7 mM aggregated Aβ_{40} stock suspension (1−50 μL). After an incubation period of 30 s, 1 mM Tris buffer (pH 7.4, 25−74 μL) was added to an Aβ_{40}−Cu(I) suspension (where necessary, the pH was further adjusted to 7.4 with 0.1 M HCl). After the sample had been mixed for 2 s, 20 mM DMPO (10 μL) was quickly added followed by 0.1 M H_2O_2 (10 μL). The final component concentrations in a total volume of 100 μL were 0.1 mM $Cu(CH_3CN)_4PF_6$, 1−140 μM Aβ_{40} aggregates, 2 mM DMPO, and 10 mM H_2O_2. The final pH value of the Aβ_{40}−Cu(I) aggregate system was 7.4 ± 0.01.

The concentration-dependent oxidant and antioxidant activity of aggregated Aβ_{40}−Cu(II) (prepared by procedure A) or Aβ_{40}−Cu(I) (prepared by procedure B) samples was determined by ESR measurements, performed 150 s after the addition of H_2O_2. All final solutions contained 5% (v/v) acetonitrile.

The time-dependent oxidant and antioxidant activity of aggregated Aβ_{40}−Cu(II) (prepared by procedure A) or Aβ_{40}−Cu(I) (prepared by procedure B) samples was also determined by ESR measurements. Specifically, the kinetics of the Cu-induced H_2O_2 decomposition modulated by aggregated Aβ_{40} was monitored for 1 h in 2−5 min intervals. Kinetic data are presented as the amount of DMPO-OH adduct, obtained by integration of the second peak of the DMPO-OH adduct quartet, versus time.

Analysis of Aβ_{40} Peptide Composition under Oxidative Conditions. Samples were prepared by adding 2 mM Cu $(CH_3CN)_4PF_6$ in acetonitrile (5 μL), 1 mM $Cu(NO_3)_2$ (10 μL), or 1 mM $FeSO_4$ (10 μL) to a 0.7 mM Aβ_{40} solution (10 μL). After an incubation period of 30 s, 1 mM NH_4HCO_3 buffer (pH 7.4, 70−75 μL) was added to Aβ_{40}−Cu/Fe complex solutions. After the sample had been mixed for 2 s, 0.1 M H_2O_2 (10 μL) was quickly added. Final component concentrations in a total volume of 100 μL were 0.1 mM $Cu(CH_3CN)_4PF_6$, $Cu(NO_3)_2$, or $FeSO_4$, 0.07 mM Aβ_{40}, and 10 mM H_2O_2. Control samples contained 0.1 mM $Cu(CH_3CN)_4PF_6$, Cu $(NO_3)_2$, or $FeSO_4$ and 0.07 mM Aβ_{40}, without H_2O_2. Altogether, there were 13 samples: (1) 0.07 mM Aβ_{40}; (2) 0.07 mM Aβ_{40} and 0.1 mM $Cu(CH_3CN)_4PF_6$ incubated for 4 min (control); (3) 0.07 mM Aβ_{40}, 0.1 mM Cu $(CH_3CN)_4PF_6$, and 10 mM H_2O_2 incubated for 4 min; (4) 0.07 mM Aβ_{40} and 0.1 mM $Cu(CH_3CN)_4PF_6$ incubated for 24 h (control); (5) 0.07 mM Aβ_{40}, 0.1 mM Cu $(CH_3CN)_4PF_6$, and 10 mM H_2O_2 incubated for 24 h; (6) 0.07 mM Aβ_{40} and 0.1 mM $FeSO_4$ incubated for 4 min (control); (7) 0.07 mM Aβ_{40}, 0.1 mM $FeSO_4$, and 10 mM H_2O_2 incubated for 4 min; (8) 0.07 mM Aβ_{40} and 0.1 mM $FeSO_4$ incubated for 24 h (control); (9) 0.07 mM Aβ_{40}, 0.1 mM $FeSO_4$, and 10 mM H_2O_2 incubated for 24 h; (10) 0.07 mM Aβ_{40} and 0.1 mM $Cu(NO_3)_2$ incubated for 21.5 min (control); (11) 0.07 mM Aβ_{40}, 0.1 mM $Cu(NO_3)_2$, and 10 mM H_2O_2 incubated for 21.5 min; (12) 0.07 mM Aβ_{40} and 0.1 mM $Cu(NO_3)_2$ incubated for 24 h (control); and (13) 0.07 mM Aβ_{40}, 0.1 mM $Cu(NO_3)_2$, and 10 mM H_2O_2 incubated for 24 h. Amino acid quantities were evaluated by amino acid analysis. Amino acid quantities in oxidized Aβ_{40} were calibrated versus hydrolysis-stable amino acids (Ala and Val). The "calibration factor" represents the quantity, in picomoles, of one hydrolytically stable

amino acid. Therefore, the calibration factor equals 100%. Aβ_{40} contains two Ala and six Val residues. The calibration factor is an average of these three amino acids in picomoles {[($Ala_{[pmol]}$/3) + ($Val_{[pmol]}$/6)]/2}. Oxidative damage to Aβ_{40} was measured by calculating the quantity of His residues in Aβ_{40}. Aβ_{40} contains three His residues; therefore, the quantity of His in the peptide was calculated by {100 × ($His_{[pmol]}$/3)/(calibration factor)}.

RESULTS

The debate on the role of Aβ_{40} under both normal physiological conditions and oxidative stress has still not been resolved. (*31*) Therefore, here, we targeted the elucidation of the role of Aβ_{40} based on monitoring its function in cell-free simulations of oxidative conditions. Specifically, we studied the modulation of Cu(I)/Cu(II)/Fe(II)-induced H_2O_2 decomposition by Aβ_{40}. We applied soluble Aβ_{40}−metal ion complexes to mimic normal physiological conditions and aggregated Aβ_{40}−metal ion complexes to simulate AD conditions. The effect of Aβ_{40} on OH radical production was quantitatively studied by ESR.

For this purpose, we prepared soluble Aβ_{40}−Cu(I)/Cu(II) aggregates and characterized them. In addition, we prepared Aβ_{40}−Cu(I)/Cu(II)/Fe(II) complexes and demonstrated their solubility. The preparation of these complexes is especially challenging as the Aβ_{40} peptide easily aggregates in the presence of metal ions (*47*).

Next, we established the ESR measurement conditions suitable for exploring both the concentration- and time-dependent modulation by Aβ_{40}.

(1) Preparation of Aβ_{40}−Cu(I)/(II)/Fe(II) Complexes and Establishment of ESR Experimental Conditions. (1.1) Preparation of Aβ_{40}−Cu(I)/(II)/Fe(II) Soluble Complexes. Several protocols for the solubilization of Aβ_{40} have been reported. These methods involve the monomerization of Aβ_{40} with strong acids [e.g., trifluoroacetic acid (TFA)] or bases (e.g., NaOH) and α-helix promoters (polar organic solvents) such as DMSO or fluorinated alcohols [hexafluoroisopropanol (HFIP), trifluoroisopropanol (TFIP), or trifluoroethanol (TFE)]. The most common methods for solubilization are use of the TFA−HFIP protocol (*48*), use of DMSO (*49*), or the "NaOH method" (*39*). In the TFA−HFIP protocol, amyloid protein is monomerized by dissolving it in TFA, followed by TFA evaporation. To avoid β-sheet formation and aggregation of Aβ_{40}, the TFA salt peptide is dissolved in HFIP which induces α-helix formation. After evaporation of the HFIP, the peptide residue is dissolved in an aqueous buffer (pH 7.4) (*48*). In the "DMSO method", Aβ_{40} is dissolved in DMSO and aliquots of this concentrated stock are diluted with an aqueous buffer (pH 7.4) (*43*,*50*).

Here, we applied the NaOH method, based on the protocol developed by Bitan and Teplow (*39*). In this method, Aβ_{40} is monomerized by dissolution in base (NaOH or NH_4OH), followed by freeze-drying. The freeze-dried NaOH salt peptide can then be dissolved in any buffer of choice, as long as the final pH is above 7. Keeping the pH above 7 is essential for avoiding isoelectric precipitation (precipitation induced due to crossing the peptide pI) (*51*).

The TFA−HFIP and DMSO protocols are less useful for the current study, since HFIP may possibly serve as a radical scavenger. Likewise, DMSO is a known radical scavenger (*52*) and, therefore, cannot be included in the ESR sample solution described below.

Although the methods described above are useful for Aβ_{40} solubilization, Aβ_{40} solubilization in the presence of Cu or Fe ions is a challenge as aggregation of Aβ_{40} is significantly enhanced in the presence of Cu or Fe ions (*43*).

Thus, to achieve soluble Aβ_{40}−Cu(I)/Cu(II)/Fe(II) complexes, we added equimolar amounts of Cu(I)/Cu(II)/Fe(II) salts to the solubilized Aβ_{40} (NaOH method) at pH ∼8. The final pH was adjusted to 7.4. These Aβ_{40}−metal ion solutions were immediately used.

(1.2) Demonstration of the Solubility of Aβ_{40} Complexes under ESR Measurement Conditions. To evaluate the solubility of Aβ_{40}−Cu(I)/Cu(II)/Fe(II) complexes, we analyzed Aβ_{40}−Cu(I)/Cu(II)/Fe(II) samples on gel (Figure 1). The analysis of the degree of solubility or aggregation of Aβ_{40}−Cu(I)/Cu(II)/Fe(II) complexes could not involve the use of denaturing PAGE, since the addition of SDS to the polyacrylamide gel (SDS−PAGE) may result in the disassembly of the Aβ_{40} aggregates, if any, on the gel.

Therefore, our analytical method of choice was the use of Native PAGE as it does not involve any denaturing factor (SDS, β-mercaptoethanol, or heating) and the proteins remain in their native folded state. Recently, Hou and Zagorski have shown, using the Native PAGE technique (7.5% polyacrylamide Tris-HCl gels, directly stained with SYPRO ruby dye), that the addition of 130 μM Cu(II)/Zn(II) ions [in phosphate buffer (pH 7.4)] to 130 μM monomeric Aβ_{40} provided monomeric Aβ_{40}−metal ion complexes (*53*).

Here, in our ESR studies, we employed Cu(I)/Fe(II) and Cu(II) in the presence of Aβ_{40} in 1 mM Tris buffer (pH 7.4). As our Aβ_{40}−metal ion complexes were different from those of Hou and Zagorski, we analyzed the composition of the samples described above by 15% polyacrylamide gels. The gels provide a resolution of 10 kDa (*54*), which in Aβ_{40} terms (MW ∼ 4 kDa) equals a dimer, and therefore serve as a good means for demonstrating Aβ_{40} solubility.

Therefore, Aβ_{40}−Cu(I)/Cu(II)/Fe(II) complexes were separated on gels, which were then stained with 0.25% Coomassie blue (R250) dye. Coomassie blue dye detects as little as 0.5 μg of protein present in a gel matrix. As the gels were loaded with samples containing ∼17.5 μg of Aβ, we assumed that the Coomassie blue staining was sufficiently sensitive to detect traces of soluble (insoluble) Aβ. In addition, the gels were stained with Sypro ruby red dye, yet this dye was less sensitive than Coomassie blue and did not stain all bands (results not shown).

To determine Aβ_{40} solubility in the ESR samples mentioned below, the gel was loaded with Aβ_{40}−Cu(I)/Cu(II)/Fe(II) complex samples. The gel samples were prepared in the same way as the ESR samples (lanes 2−4 of Figure 1A) and electrophoresed versus two controls: soluble Aβ_{28}−Cu(I) complex and soluble Aβ_{40} (lanes 1 and 5, respectively, of Figure 1A). Evidence of the solubility of Aβ_{40}−Cu/Fe complexes was obtained by

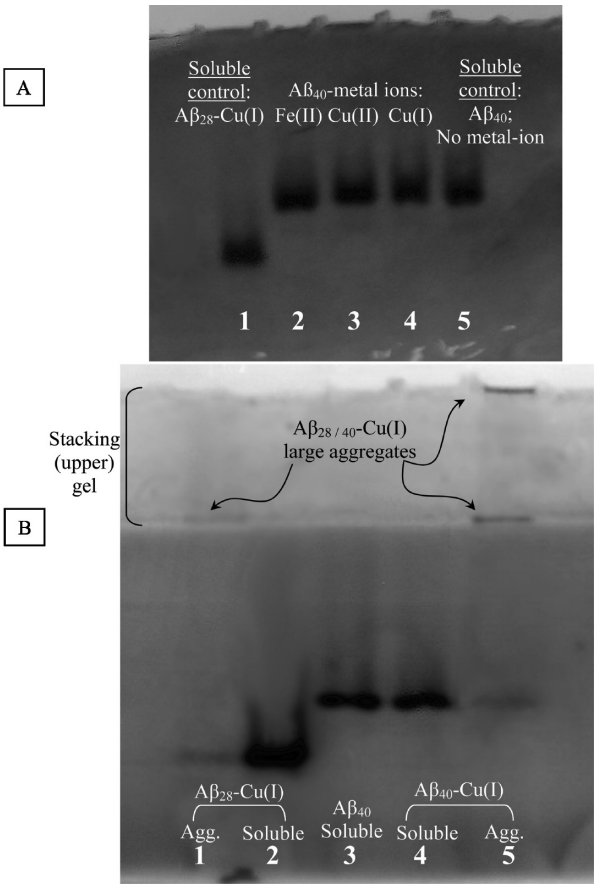

FIGURE 1: Characterization of soluble Aβ_{40}−Cu(I)/Cu(II)/Fe(II) complexes by Native PAGE. The 15% Tris-HCl gels were loaded with 25 μL samples and electrophoresed for 1.5 h at 100 V. The native gels were directly stained with Coomassie blue (R250). All manipulations were performed at 4 °C (all mentioned concentrations are final). (A) Soluble A$\beta_{28/40}$−metal ion complexes: lane 1, control containing soluble Aβ_{28}−Cu(I), prepared by adding 0.1 mM $Cu(CH_3CN)_4PF_6$ to 0.06 mM Aβ_{28}; lanes 2−4, samples containing soluble Aβ_{40}−Cu(I)/Cu(II)/Fe(II) complexes prepared by mixing 0.11 mM $FeSO_4$/$Cu(NO_3)_2$/$Cu(CH_3CN)_4PF_6$ with 0.126 mM Aβ_{40}; and lane 5, control containing 0.161 mM soluble Aβ_{40} without a metal ion. (B) Soluble vs aggregated A$\beta_{28/40}$−Cu(I) complexes: lane 1, control containing aggregated Aβ_{28}−Cu(I) complex prepared by mixing 0.2 mM $Cu(CH_3CN)_4PF_6$ and 0.36 mM Aβ_{28} (pH adjusted to ~7.5 with 0.025 M NaOH and the sample incubated for 1 month at room temperature); lane 2, control containing soluble Aβ_{28}−Cu(I) complex prepared as described above; lane 3, control containing 0.161 mM soluble Aβ_{40} without a metal ion; lane 4, sample containing soluble Aβ_{40}−Cu(I) complex prepared as described above; lane 5, sample containing aggregated Aβ_{40}−Cu(I) complex prepared by mixing 0.2 mM $Cu(CH_3CN)_4PF_6$ with 0.14 mM Aβ_{40}. The pH of the solutions was then acidified to 1 and quickly neutralized to 7.5. This mixture was then incubated at room temperature for 3 days.

staining and comparing the following lanes. (1) The bands of Aβ_{40}−metal ion complexes (lanes 2−4) were aligned with the soluble Aβ_{40} band (lane 5). This alignment implies that metal ion coordination to Aβ_{40} does not alter the peptide solubility under ESR measurement conditions. (2) Additional evidence of the solubility of the Aβ_{40}−Cu(I) complex is provided by comparison of the Aβ_{40}−Cu(I) complex (lane 4) to the soluble Aβ_{28}−Cu(I) complex (lane 1) (*36*). The soluble Aβ_{28}−Cu(I) complex migrates further because of its smaller size.

For comparison of aggregated versus soluble Aβ_{40} complexes, the gel was loaded with (1) soluble Aβ_{28}−Cu(I) and Aβ_{40}−Cu(I) samples (lanes 2 and 4, respectively, of Figure 1B), (2) control of soluble Aβ_{40} (lane 3 of Figure 1B), and (3) aggregated controls: Aβ_{28}−Cu(I) aggregates matured over 1 month (lane 1 of Figure 1B) and Aβ_{40}−Cu(I) aggregates which were isoelectrically aggregated and matured over 3 days (*40*) (lane 5 of Figure 1B). The aggregated A$\beta_{28/40}$−Cu(I) samples contained a minute fraction of soluble A$\beta_{28/40}$−Cu(I) complex (lanes 1 and 5), aligned with the soluble A$\beta_{28/40}$−Cu(I) band (lanes 2 and 4). However, a closer inspection of the stacking gel (top gel) showed the presence of A$\beta_{28/40}$−Cu(I) aggregates (lanes 1 and 5) that were too large to migrate in the gel and became stuck in the top gel.

The resolving gel (bottom gel) contained 15% acrylamide. A degree of polymerization of 10−15% resolves 10−80 kDa proteins on the native gel (*54*). Thus, proteins larger than 80 kDa will not migrate to the resolving gel and will remain in the stacking gel. No bands were observed in the top gel for lanes 2 and 4, thus indicating that there are no aggregates in these samples and they contain only soluble A$\beta_{28/40}$−Cu(I) complex.

The stacking gel contains 4−5% acrylamide, and this degree of polymerization resolves proteins of > 100 kDa (*54*). Thus, proteins larger than 100 kDa will not penetrate the stacking gel. The Aβ_{40}−Cu(I) aggregates contained also a high-molecular mass fraction of ≥100 kDa, which remained in the well and did not migrate at all during the electrophoresis (lane 5).

(1.3) Selection of ESR Measurement Conditions. ESR was our method of choice for monitoring the effect of Aβ_{40} on the production of •OH from Cu/Fe-induced H_2O_2 decomposition. For the detection of OH radicals, we applied DMPO as a spin trap. The optimized ESR measurement conditions applied here are based on our former study on the modulation of OH radical production in Cu/Fe-H_2O_2 systems by Aβ_{28} (*36*). Briefly, we selected the ESR measurement conditions as follows. **(A) Selection of Redox-Active Metal Ions.** Cu(II) and Fe(III) found in high concentrations in amyloid plaques (*5*) are easily reduced to Cu(I) and Fe(II), respectively, in the presence of A$\beta_{40/42}$. Cu(I) and Fe(II) were proposed to cause oxidative damage (*23*). Therefore, we studied here both Cu(I)− and Fe(II)−Aβ_{40} complexes. Cu(I) salt was dissolved in acetonitrile [the final acetonitrile concentration in Cu(I)-containing ESR samples was 5% (v/v)] which serves as a Cu(I) stabilizing ligand against oxidation to Cu(II). In addition, we studied the Cu(II)−Aβ_{40} complex, as Cu(II) induces OH radical production through a Haber−Weiss-like reaction (eqs 1−4) (*21*). We have not studied Fe(III) ions, because under our ESR experimental conditions, we did not observe any DMPO-OH adduct in the presence of Fe(III) and H_2O_2. **(B) Metal Ion Concentration.** In Aβ plaques, the Cu concentration was measured to be ~0.4 mM (*5*). Therefore, in our studies, we used Cu(I)/Cu(II)/Fe(II) concentrations on the same order of magnitude, 0.1 mM. **(C) Aβ_{40} Concentration.** We studied Aβ_{40} at nanomolar to micromolar concentrations (7 nM to 350 μM), which correspond to Aβ biological concentrations ranging from nanomolar concentrations in healthy individuals to micromolar concentrations under oxidative stress conditions (*33*,*34*). **(D) Buffer and pH.** ESR samples were

prepared in 1 mM Tris buffer (pH 7.4). Tris may be a radical scavenger; however, at a concentration of 1 mM, its scavenging effect is minimal (*55*). In addition, the Tris buffer has a stabilizing effect; namely, it prevents the formation of metal ion oxides (even at pH 7.4) by acting as a metal ion chelator (*56*). Cu(I) oxide formation was prevented also due to the addition of acetonitrile [5% (v/v)] to the solution. **(E) DMPO (spin trap) Concentration.** The extent of DMPO-OH adduct formation was linearly increased with the addition of DMPO to Cu(I/II)/Fe(II)−H_2O_2 solutions at concentrations up to ~15−20 mM, while exceeding these concentrations resulted in a constant DMPO-OH concentration (data not shown). The DMPO concentration should be as low as possible to avoid competition between the tested Aβ-metal-ion complex and DMPO. We used 2 mM DMPO throughout all ESR measurements. This DMPO concentration is sufficiently large to enable the detection of DMPO-OH signals.

(1.4) Determination of the Oxidation State of Cu in ESR Samples. To confirm that the Cu ion in the Aβ_{40}−Cu(I) soluble complex remains in the +1 oxidation state throughout the ESR measurements, we analyzed this complex by UV spectroscopy and the Cu(I)-specific indicator, BCA. Soluble Aβ_{40}−Cu(I) samples were analyzed by UV, 5 min and 3 days after preparation. No Cu(II) ions could be detected, and the Cu(I) concentration did not change in the presence of soluble Aβ_{40} even after 3 days (at pH 7.4 and room temperature in a closed Eppendorf tube), thus verifying the composition of the Aβ_{40}−Cu(I) complex in ESR measurements.

(2) Concentration-Dependent Modulation of OH Radical Formation by Soluble Aβ_{40}. To compare the activity of the endogenous Aβ_{40} to that of Aβ_{28}, which we investigated previously (*36*), we studied the modulatory function of Aβ_{40} in the same OH radical-producing systems.

For this purpose, we added 0.1 mM Fe(II), Cu(II), or Cu(I) to Aβ_{40} solutions in the concentration range from 7 nM to 0.35 mM. Then, DMPO was added, followed by H_2O_2, and the concentration of the formed OH radicals in these systems was evaluated by ESR measurements as a percent of control (Figure 2).

Previously, we showed that Aβ_{28} inhibited Cu(I/II)/Fe(II) ion-induced H_2O_2 decomposition, resulting in an Aβ_{28} concentration-dependent sigmoidal decay of OH radical formation (*36*). However, here, the pattern of Aβ_{40} concentration-dependent inhibition was in the form of an exponential decay (Figure 2). Specifically, at 0.6 nM to 36 μM Aβ_{28}, no significant inhibition of radical formation was observed, while with Aβ_{40}, a decrease in the •OH concentration was observed already at ca. 0.7 μM Aβ_{40} for Cu(I)/Fe(II) systems (Figure 2, inset). Aβ_{40} inhibited both Cu(I)- and Fe(II)-induced H_2O_2 decomposition with similar IC_{50} values, 15.5 and 13.0 μM, respectively (Table 1). For the sake of comparison, soluble Aβ_{28} inhibited the Cu(I) and Fe(II)-H_2O_2 systems with IC_{50} values of 59 and 84 μM, respectively (*36*).

Soluble Aβ_{40} had a different mode of activity in the Cu(II)-H_2O_2 system. A pro-oxidant phase, up to 150% of control, was observed at low Aβ_{40} concentrations [0.7−30 μM, at 0.1 mM Cu(II)], and an antioxidant phase was observed at higher concentrations (30−280 μM) (Figure 2). Previously, we observed a similar biphasic pattern

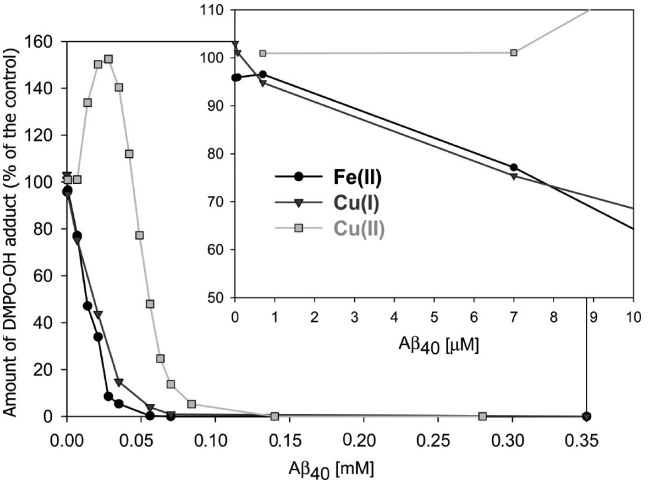

FIGURE 2: Modulation of the Cu(I)/Cu(II)/Fe(II)-induced H_2O_2 decomposition by the soluble Aβ_{40} peptide. The reaction was performed in a 1 mM Tris buffer, containing 0.1 mM $FeSO_4$, Cu$(CH_3CN)_4PF_6$, or Cu$(NO_3)_2$, 10 mM H_2O_2, 2 mM DMPO (pH 7.4), and 0−0.35 mM Aβ_{40} peptide. The final Cu(I)−Aβ_{40}−H_2O_2 solution contained 5% (v/v) acetonitrile. The amount of DMPO-OH adduct formed under these conditions is given as the percentage of control, which contains Cu$(CH_3CN)_4PF_6$, $FeSO_4$, or Cu$(NO_3)_2$, H_2O_2, and DMPO. The curves represent the average of two experiments. The *x*-axis has units of millimolar Aβ_{40}, and the inset has units of micromolar Aβ_{40}.

for the modulation of the Cu(II)-H_2O_2 system by nucleotides and inorganic phosphates (*46*). Soluble Aβ_{40} inhibited Cu(II)-induced H_2O_2 decomposition, with an IC_{50} value of 62 μM, equipotent to Aβ_{28} (IC_{50} value of 61 μM) (*36*). The IC_{50} of Aβ_{40} was not altered from that of the shorter Aβ_{28} peptide, but the modulation pattern changed from a sigmoidal decay for Aβ_{28} to a biphasic modulation for Aβ_{40}.

(3) Mechanism of Inhibition of OH Radical Formation by Aβ_{40}: Metal Ion Chelation versus Radical Scavenging. The high antioxidant activity of Aβ_{40} may be due to two mechanisms: metal ion chelation and radical scavenging.

To explore the possible mechanism of modulation of radical formation by Aβ_{40}, we incubated soluble Aβ_{40} and Cu(I), Cu(II), or Fe(II), with or without H_2O_2, and monitored any changes in the amino acid composition of the Aβ_{40}−Cu(I)/Fe(II) complex after 4 min (ESR measurement time) or 24 h at pH 7.4 and room temperature, and for 21.5 min (ESR measurement time) or 24 h for the Aβ_{40}−Cu(II) complex at pH 7.4 and room temperature. Aβ_{40} samples in Cu/Fe-H_2O_2 solutions were evaluated by an amino acid analyzer and compared to Aβ_{40} samples containing Cu/Fe ions in the absence of H_2O_2. These control samples are required as Cu/Fe ions create an oxidative environment by inducing the formation of H_2O_2 from atmospheric oxygen.

The quantity of any degraded amino acid residue found in each sample is presented as a percentage of the calibration factor. The calibration factor represents 100% amino acid quantity for a given sample (Table 2). For example, in the sample containing only Aβ_{40}, the quantity of histidine was 102%; in other words, histidine was intact.

A significant amount of Aβ_{40}'s histidine was degraded as compared to Aβ_{28}'s histidine under ESR experimental conditions (Table 2). Specifically, almost none of Aβ_{40}'s histidine degradation was observed in the presence of Cu

Table 1: Inhibition of Metal Ion-Induced OH Radical Production by Soluble or Aggregated Aβ_{40} at pH 7.4[a]

metal ion	IC_{50} (μM)[b] of soluble Aβ_{40}	IC_{50} (μM)[b] of aggregated Aβ_{40}	IC_{50} (μM)[b] of soluble Aβ_{28} (*36*)	IC_{50} (μM)[b] of Trolox
Cu(I)	15.5 ± 1.5	16.3 ± 1.02	58.6 ± 2.6	650 ± 110 (*46*)
Cu(II)	61.9 ± 9.7	50.5 ± 1.01	60.6 ± 0.5	na[c]
Fe(II)	13.0 ± 1.9	–	83.9 ± 6.1	200 ± 2 (*87*)

[a] IC_{50} values represent Aβ_{40} concentrations that inhibit 50% of the OH radical production from decomposition of H_2O_2, catalyzed by 0.1 mM Cu(I)/Cu(II) or Fe(II) ions. [b] IC_{50} values were obtained from fitting the Aβ_{40} data to a three-parameter exponential curve, with errors being taken as the deviation from the average value. [c] The DMPO-OH adduct decomposes in the presence of Cu(II) and Trolox, and the IC_{50} value could not be evaluated.

Table 2: Aβ_{40} Radical Scavenging Activity Monitored by Amino Acid Analysis[a]

	% of loss of amino acid in Aβ					
	Aβ_{40}				Aβ_{28} (*36*)	
sample	His loss	Tyr loss	His loss	Phe loss	His loss	Tyr loss
only Aβ	0	0	0	0	0	0
Aβ−Cu(I), 4 min	6.67	11.20	1.96	2.46	5.07	5.82
Aβ−Cu(I)-H_2O_2, 4 min	93.16	78	40.69	27.74	25.74	32.44
Aβ−Cu(I), 24 h	7.65	13.40	3.40	3.00	10.16	21.28
Aβ−Cu(I)-H_2O_2, 24 h	100	100	59.90	34.60	50.78	64.21
Aβ−Fe(II), 4 min	1.32	15.43	0	2.46	15.64	13.68
Aβ−Fe(II)-H_2O_2, 4 min	93.50	100	44.62	35.61	18.43	26.25
Aβ−Fe(II), 24 h	2.67	11.96	0	2.83	20.15	16.52
Aβ−Fe(II)-H_2O_2, 24 h	94.13	83.85	41.74	27.45	37.26	40.38
Aβ−Cu(II), 21.5 min	0	0	0	0.37	2.15	6.09
Aβ−Cu(II)-H_2O_2, 21.5 min	30.87[b]	19.61	2.86	4.72	37.01	49.06
Aβ−Cu(II), 24 h	0.55	0	0	0.77	3.68	6.74
Aβ−Cu(II)-H_2O_2, 24 h	70.28[c]	22.45	4.23	5.70	77.44	79.27

[a] Values represent the percentage of loss of His residues in 0.7 mM soluble Aβ_{40} at pH 7.4 in 1 mM NH_4HCO_3. Aβ_{40}-scavenged OH radicals produced from the decomposition of H_2O_2 catalyzed by 0.1 mM Cu(I)/Cu(II) or Fe(II) ions. [b] A level of 40% His oxidation was found by Atwood et al. in Aβ_{40}−Cu(II)-H_2O_2 samples after 1 h (*66*). [c] A level of 79% His oxidation was found by Atwood et al. in Aβ_{40}−Cu(II)-H_2O_2 samples after 24 h (*66*).

(I)/Fe(II) or Cu(II), without H_2O_2, after 4 or 21.5 min, respectively. However, the addition of H_2O_2 to the samples, under the same conditions (after a 4 min incubation period), resulted in 93.16 or 93.50% His loss for Cu(I)- or Fe(II)-containing samples, respectively. A 30.87% His loss was observed after incubation of Aβ_{40} and Cu(II) with H_2O_2 for 21.5 min.

Likewise, during a prolonged incubation of Aβ_{40} with Cu(I), Fe(II), and Cu(II) for 24 h without the addition of H_2O_2, we observed only a slight degradation of His residues (7.65, 2.67, and 0.55%, respectively). However, the addition of H_2O_2 to the samples and incubation for 24 h resulted in an almost complete loss of His: 100, 94.13, and 70.28% for Cu(I), Fe(II), and Cu(II)-H_2O_2, respectively.

As we observed before for Aβ_{28} (*36*), Aβ_{40} also underwent a significant His oxidation, upon prolonged incubation times (24 h). However, during short incubation times [4 min (Table 2)], in the presence of Cu(I) or Fe(II) ions, Aβ_{40} appears to be a significantly better radical scavenger than Aβ_{28}, yet in the presence of Cu(II) ions (after either 21 min or 24 h), there is only a minimal difference in the His loss percentage between Aβ_{28} and Aβ_{40}.

Aβ_{40}'s Tyr10 was oxidized to approximately the same extent as His residues [especially in Cu(I)/Fe(II) systems (Table 2)], implying that Tyr10 coordinates with the metal ion. Indeed, the Cu(II) ion was found (by S-band ESR) to bind Aβ_{40} with a 3N1O coordination, and the oxygen atom donor ligand was proposed to be either Tyr10 (*7*) or Asp1 (*57*). Our results, showing extensive Tyr oxidation, support the proposed Tyr10 binding as the fourth ligand for the Cu(I)/Fe(II) ion (*7*).

To elucidate if histidine oxidation was due to a direct metal ion binding to histidine or to a nonspecific oxidation, we calculated the percentages of oxidation of all other Aβ_{40} amino acids. Only minor oxidation (0−15%) was observed for Aβ_{40}'s amino acids other than His and Tyr. This finding indicates that there is no nonspecific oxidation, and it is mostly the Cu/Fe-coordinating amino acids that suffer oxidative damage.

However, a level of oxidation of >15% was detected also for Lys and Phe in Cu(I)/Fe(II)-H_2O_2 systems (Table 2). Aβ_{40} has two lysine residues (Lys16 and Lys28) and three phenylalanine residues (Phe4, Phe19, and Phe20). A loss of 40.69−59.90% of Lys residue indicates that at least one of the two Lys residues of Aβ_{40} (possibly Lys16) is in the proximity of the metal ion (Scheme 1). The percentage of Phe residue oxidation is 27.45−35.61% in the presence of Cu(I)/Fe(II) and H_2O_2, indicating that one of the three Phe residues, possibly Phe4, is near the complex core and is oxidized (Scheme 1). Minor oxidation is also observed for Arg5 (15.0−31.48%) and for Glu (Glu3, Glu11, and Glu22) and Gln15 residues (15.0−24.0%) in the presence of Cu(I)/Fe(II) and H_2O_2.

However, in the presence of Cu(II) ion, only His residues and Tyr10 were oxidized, implying that the Aβ_{40}−Cu(II)-H_2O_2 system produces radicals to a lesser

Scheme 1: Proposed Coordination of Cu/Fe Ions to the Aβ Peptide Based on Amino Acid Analysis of (A) Aβ_{28}−Cu(I/II)/Fe(II) Complexes and (B) Aβ_{40}−Cu(I/II)/Fe(II) Complexes

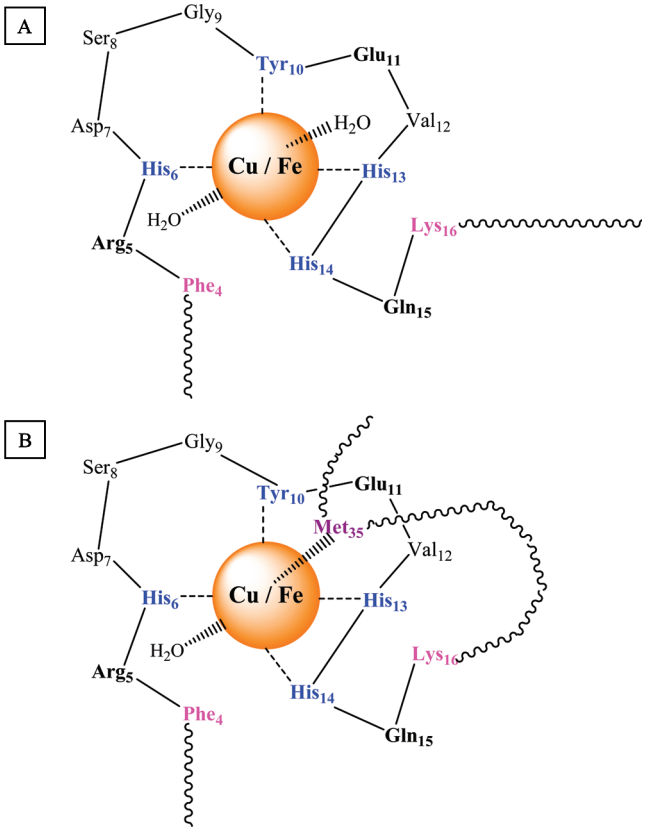

extent than the Aβ_{40}−Cu(I)/Fe(II)-H_2O_2 system. Indeed, in a previous study, we showed that the Cu(II)-H_2O_2 system produces OH radicals significantly more slowly than the Cu(I)-H_2O_2 system (*46*).

(4) Time-Dependent Modulation of OH Radical Formation by Soluble Aβ_{40}. We next studied the time-dependent modulation of $^{\bullet}$OH production by soluble Aβ_{40} (Figures 3 and 4). In the Cu(I)- and Fe(II)-H_2O_2 systems, where OH radicals are instantaneously produced via Fenton chemistry, we observed only the exponential decay of the DMPO-OH adduct versus time (Figure 3, control). Likewise, in the presence of Aβ_{40}, we observed an exponential decay of the DMPO-OH adduct. For instance, at 30 μM Aβ_{40} in the Fe(II)-H_2O_2 system, the DMPO-OH adduct concentration was completely diminished after 20 min (Figure 3B). We made similar observations with Aβ_{28} (*36*).

However, in the Cu(II)-H_2O_2 system (control), we observed a time-dependent increase in OH radical production (Figure 4). This time-dependent modulation of the DMPO-OH concentration appeared also in the presence of Aβ_{40}, yet Aβ_{40} reduced significantly the $^{\bullet}$OH concentration as compared to the control. This finding is similar to our previous results with Aβ_{28} (*36*).

(5) Modulation of OH Radical Formation by Aβ_{40} Aggregates. Previously, we showed that aggregated Aβ_{28} was a less potent inhibitor of $^{\bullet}$OH formation than soluble Aβ_{28} (*36*). Therefore, here, we studied also the modulatory function of aggregated Aβ_{40} in the oxidative systems mentioned above.

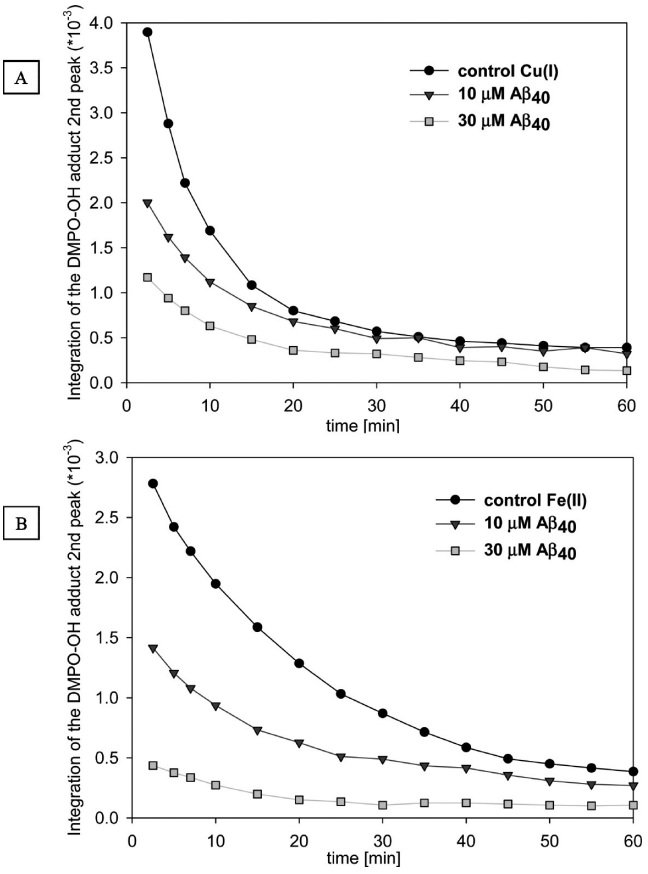

FIGURE 3: Time-dependent curves for the amount of DMPO-OH adduct generated in (A) Cu(I)-induced H_2O_2 decomposition and (B) Fe(II)-induced H_2O_2 decomposition. Reactions were performed by the addition of 10 mM H_2O_2 to solutions containing 0.1 mM $Cu(CH_3CN)_4PF_6$ or $FeSO_4$, 2 mM DMPO, and 1 mM Tris buffer (pH 7.4) in the presence of 10−30 μM soluble Aβ_{40}. The zero time point was the H_2O_2 addition time as described in Experimental Procedures. The final Cu(I) system solution contained 5% (v/v) acetonitrile.

(5.1) Preparation of Aβ_{40}−Cu(I/II) Aggregates. Metal ions were found at high concentrations in Aβ_{40} aggregates (*5*). However, it is still unknown if soluble Aβ_{40} aggregates as a complex with metal ions or mature Aβ_{40} aggregates serve as a metal ion sink. Therefore, here we prepared Aβ_{40}−metal ion aggregates in two ways: (A) inducing aggregation based on isoelectric precipitation of soluble Aβ_{40} in the presence of metal ions, followed by maturation for several days, and (B) aggregation of Aβ_{40} based on isoelectric precipitation, followed by soaking the matured aggregates with a metal ion solution.

The aggregation of Aβ_{40} was reported to occur upon incubation in 10 mM Tris-HCl (pH 7.4) at 37 °C for 1−4 days (*58*). Aggregation can be accelerated by acidifying the solution, based on isoelectric precipitation (*51*). Here, we produced 1:1 Aβ_{40}−Cu(I) aggregates by methods A and B. In method A, we quickly acidified the Aβ_{40} solution containing Cu(I) salt from pH ~8 to 1, then adjusted the solution pH to 7.4, and finally incubated the solution for 3 days at room temperature. Alternatively, Aβ_{40}−Cu(I) aggregates were prepared by method B. We prepared an Aβ_{40} aggregate suspension by acidifying the soluble Aβ_{40} solution from pH ~8 to 1, adjusting the solution pH to 7.4, and incubating the solution for 3 days

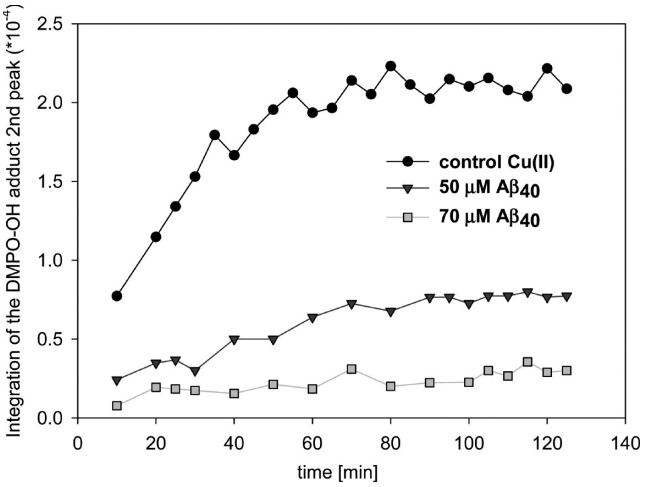

FIGURE 4: Time-dependent curves for the amount of DMPO-OH adduct generated in Cu(II)-induced H_2O_2 decomposition. Reactions were performed by the addition of 10 mM H_2O_2 to solutions containing 0.1 mM $Cu(NO_3)_2$, 2 mM DMPO, and 1 mM Tris buffer (pH 7.4) in the presence of 50−70 μM soluble Aβ_{40}. The zero time point was the H_2O_2 addition time as described in Experimental Procedures.

at room temperature. Then, an equimolar amount of Cu (I) solution was added to the Aβ_{40} aggregate suspension.

(5.2) Characterization of 1:1 Aβ_{40}−Cu(I/II) Aggregates. The Aβ_{40}−Cu aggregates prepared using methods A and B were first analyzed by UV spectroscopy to determine the Cu oxidation state. Specifically, we added a BCA indicator to Aβ_{40}−Cu aggregates [0.1 mM Aβ_{40} with 0.1 mM Cu(I)] prepared by method A. We found that after a 3 day maturation period of the Aβ_{40}−Cu(I) aggregates, all of the Cu ions were oxidized to Cu(II) ions, as indicated by disappearance of the Cu(I)−BCA peak at 560 nm and the appearance of a new band at 368 nm. However, the addition of the BCA indicator to Aβ_{40}−Cu aggregates prepared by method B [0.1 mM Cu(I) added to 0.1 mM Aβ_{40} fibrils that had matured for 3 days] resulted in the typical Cu(I)−BCA peak at 560 nm, indicating that fibrils prepared according to method B contained solely Cu(I) ions.

Aβ_{40}−Cu(I/II) aggregates prepared using methods A and B were also characterized to demonstrate fibril formation. An amyloid fibril is characterized by several criteria, including electron microscopy demonstration of fine nonbranching fibers and UV spectral evidence of the presence of a characteristic β-sheet structure using specific dyes (*59*).

We characterized Aβ_{40}−Cu(II) aggregates via Congo red dye, TEM, and ICP analysis. (I) For the Congo red (CR) dye method, Congo red specifically stains amyloid fibrils with a β-sheet secondary structure. The intensity of the dye signal (detected by UV spectroscopy) is enhanced upon binding to β-sheet fibrils (*44*,*45*,*60*). CR was added to the aggregates formed by method A and incubated for 1 or 3 days at room temperature (Figure 5). There was a minor enhancement of the CR signal in the presence of Aβ_{40}−Cu(II) aggregates that had matured for 1 day. We observed only a slight shift, of 5 nm, of the maximum absorption wavelength of the CR−Aβ_{40}−Cu(II) complex relative to CR (Figure 5A). The minor changes observed in the CR signal upon binding of Aβ_{40}−Cu(II) aggregates imply that after aggregation for 1 day the 1:1 Aβ_{40}−Cu

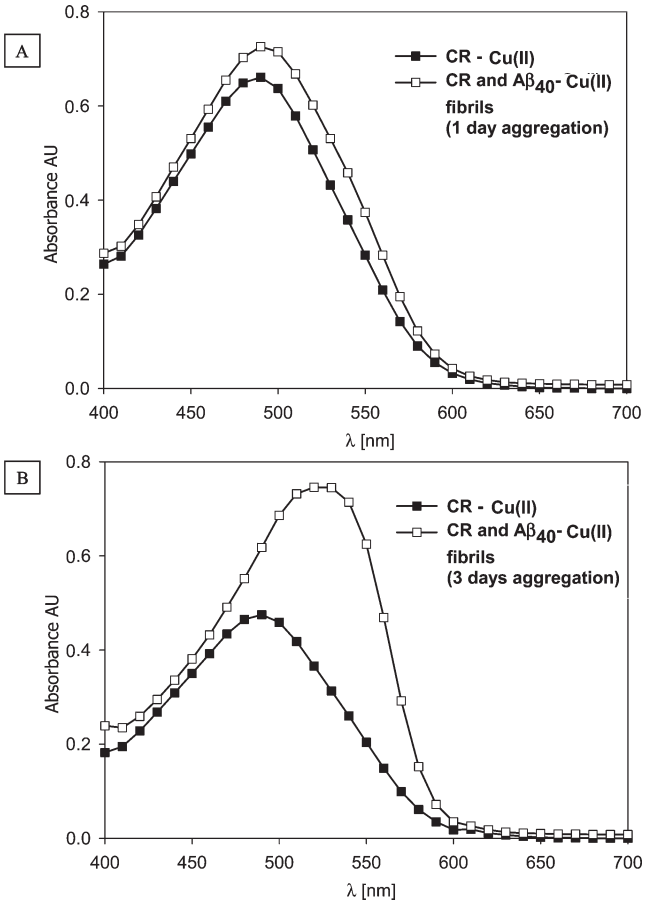

FIGURE 5: Aβ_{40}−Cu(II) fibril dye binding assay. Absorbance spectra of 20 μM Congo red (CR) and 30 μM $Cu(NO_3)_2$ in PBS (pH 7.4) in the absence or presence of Aβ_{40} fibrils. Fibrils were allowed to mature at room temperature for 1 day (A) or 3 days (B).

(II) complex has a premature fibril structure. However, the addition of CR to 3-day-matured 1:1 Aβ_{40}−Cu(II) aggregates showed a typical β-sheet mature fibril structure. This was indicated by the large enhancement of the absorption, and a 37 nm red shift of the maximum absorption wavelength of the CR−Aβ_{40}−Cu(II) complex, relative to that of CR (Figure 5B).

The addition of CR to 3-day-matured 1:1 Aβ_{40}−Cu(I) aggregates prepared by method B yielded results similar to those of Aβ_{40}−Cu(II) aggregates with a 35 nm red shift of the maximum absorption wavelength of the CR−Aβ_{40}−Cu(I) complex relative to that of CR (results not shown). However, the CR−Aβ_{40}−Cu(II) complex prepared by method A had a 0.272 AU enhancement of the maximum absorption relative to that of CR, while the CR−Aβ_{40}−Cu(I) complex, prepared by method B, had an only 0.150 AU enhancement of the maximum absorption relative to that of CR.

(II) For TEM measurements, TEM images of 1:1 Aβ_{40}−Cu(II) aggregates prepared by method A and allowed to mature for 3 days exhibited rodlike aggregates (length, 328.24 ± 67.87 nm; diameter, 17.92 ± 6.04 nm) (Figure 6A). In most cases, the rods further stacked to form larger clusters ranging from 287 to 927 nm in size (length, 611.99 ± 327.45 nm; diameter, 124.14 ± 39.69 nm) (Figure 6B). These results are consistent with previously reported data for A$\beta_{40/42}$ fibrils (*61*,*62*).

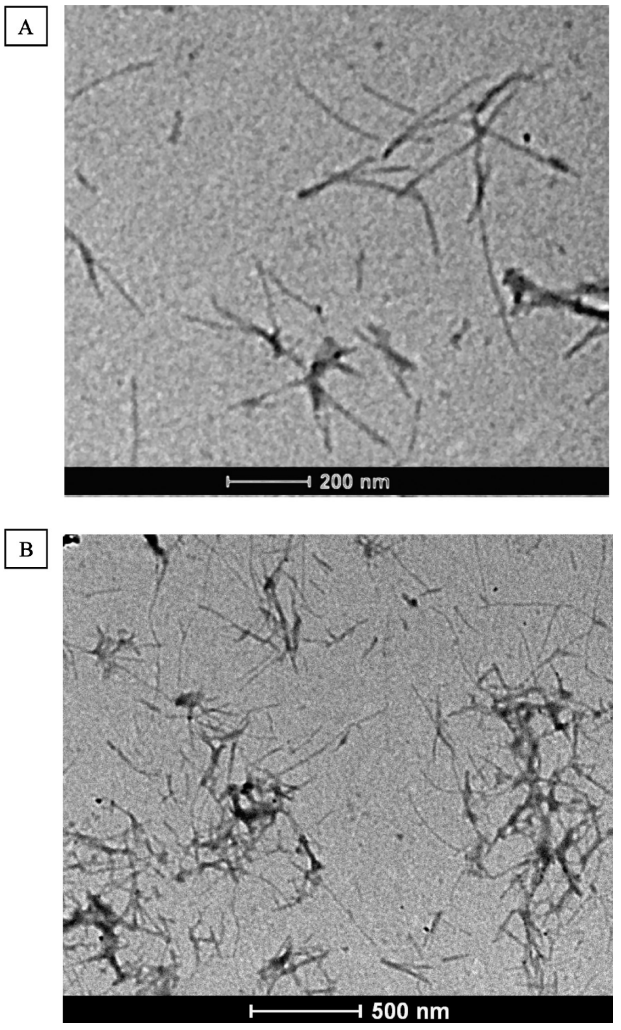

FIGURE 6: TEM images of the Aβ_{40}−Cu(II) aggregates: (A) 328.24 ± 67.87 nm fibrils and (B) 611.99 ± 327.45 nm clusters. The aggregates were prepared by method A as described in Experimental Procedures. Aβ samples were allowed to mature for 3 days at room temperature.

To find whether free Cu(II) ions were present in the aggregated samples, we filtered the Aβ_{40}−Cu(II) aggregates from the sample suspension and analyzed the filtrate by (III) ICP measurement. No free Cu ions were detected under our ESR measurement conditions with aggregated Aβ_{40}−Cu(II) samples.

(5.3) Concentration-Dependent Modulation of OH Radical Production by the Aggregated Aβ_{40}−Cu(I/II) Complex. We also studied by ESR the modulatory function of the aggregated Aβ_{40}−Cu(II/I) complex (prepared by methods A and B, respectively) in OH radical-producing systems (Figures 7 and 8).

The Aβ_{40} aggregates inhibited Cu(II)-induced H_2O_2 decomposition in a concentration-dependent manner with an exponential decay of DMPO-OH adduct concentration (Figure 7). Specifically, at concentrations of 1−45 μM Aβ_{40} aggregate, enhanced production of DMPO-OH adduct as compared to control (a pro-oxidant phase) was observed, while at concentrations of 45−105 μM Aβ_{40} aggregate, the DMPO-OH adduct concentration was decreased with an IC_{50} value of 50.5 μM (Table 1). This IC_{50} value is similar to the value of soluble Aβ_{40} in the Cu(II)-H_2O_2 system (62 μM).

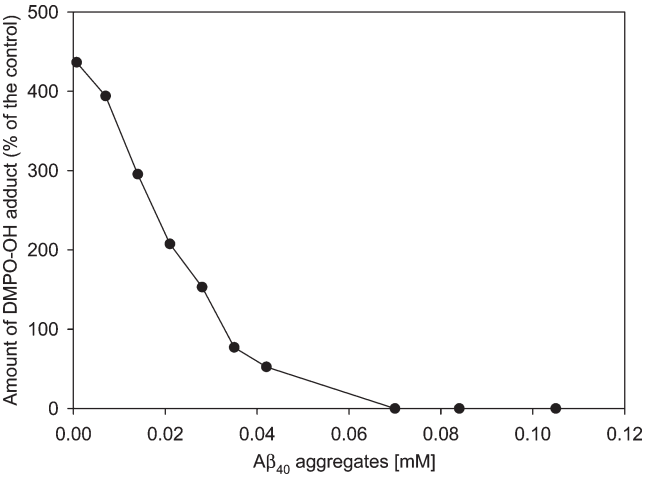

FIGURE 7: Modulation of the Cu(II)-induced H_2O_2 decomposition by 3-day-old 1−105 μM Aβ_{40}−Cu(II) aggregates prepared by method A at pH 7.4. H_2O_2 (10 mM) and DMPO (2 mM) were added to the samples, and the amount of DMPO-OH adduct was determined by ESR measurements. The amount of DMPO-OH adduct formed under these conditions is given as the percentage of control, which contains $Cu(NO_3)_2$, H_2O_2, and DMPO. The curve represents the average of two experiments.

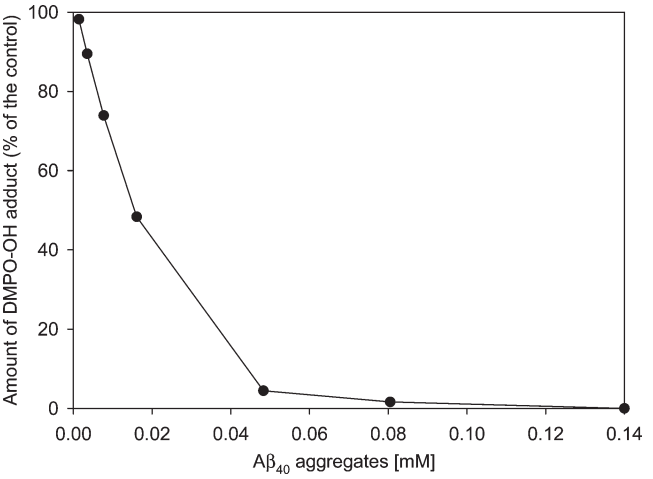

FIGURE 8: Modulation of the Cu(I)-induced H_2O_2 decomposition by Aβ_{40} aggregates prepared by method B. Aβ_{40} aggregates at a concentration of 0−0.14 mM were added to a 0.1 mM Cu$(CH_3CN)_4PF_6$ acetonitrile solution and 1 mM Tris buffer (pH 7.4). The final Aβ_{40}−Cu(I)-H_2O_2 solution contained 5% (v/v) acetonitrile. H_2O_2 (10 mM) and DMPO (2 mM) were added to the samples, and the amount of DMPO-OH adduct was determined by ESR measurements. The amount of DMPO-OH adduct formed under these conditions is given as the percentage of control, which contains Cu$(CH_3CN)_4PF_6$, H_2O_2, and DMPO. The curve represents the average of two experiments.

In addition, we evaluated the antioxidant function of aggregated Aβ_{40}−Cu(I) complexes, prepared by method B (Figure 8). The Aβ_{40} aggregates inhibited production of OH radicals from Cu(I)-induced H_2O_2 decomposition in a concentration-dependent manner with an exponential decay of the amount of DMPO-OH (Figure 8). However, here, unlike the Aβ_{40}−Cu(II)-H_2O_2 system, we did not observe any pro-oxidant phase at 1−140 μM Aβ_{40}. The IC_{50} value of Aβ_{40} aggregates was 16.3 μM, which is similar to the IC_{50} value of soluble Aβ_{40} in the Cu(I)-H_2O_2 system (15.5 μM).

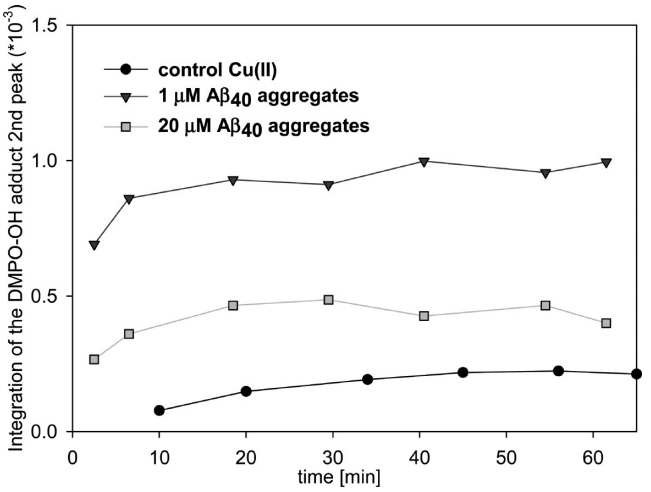

FIGURE 9: Time-dependent curves for the amount of DMPO-OH adduct generated by H_2O_2 decomposition by 1 and 20 μM Aβ_{40}−Cu (II) aggregates prepared by method A at pH 7.4. H_2O_2 (10 mM) and DMPO (2 mM) were added to the samples, and the amount of DMPO-OH adduct was monitored by ESR measurements for 60 min. The zero time point was the H_2O_2 addition time, as described in Experimental Procedures.

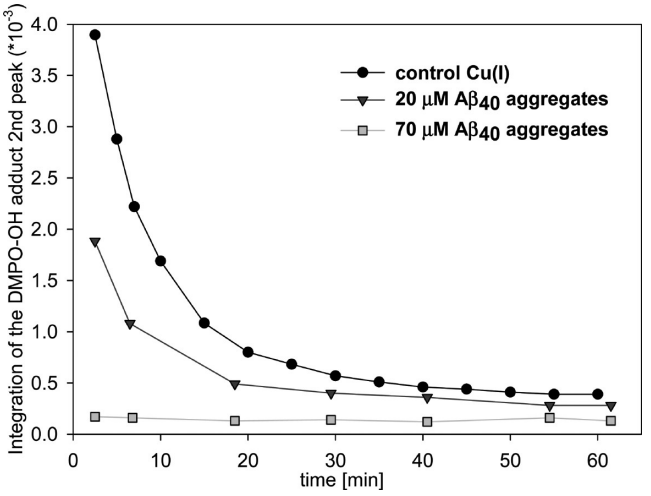

FIGURE 10: Time-dependent curves for the amount of DMPO-OH adduct generated by H_2O_2 decomposition by Aβ_{40} aggregates prepared by method B. An Aβ_{40} concentration of 20−70 μM was added to a 0.1 mM $Cu(CH_3CN)_4PF_6$ acetonitrile solution and 1 mM Tris buffer (pH 7.4). The final Aβ_{40}−Cu(I)-H_2O_2 solution contained 5% (v/v) acetonitrile. H_2O_2 (10 mM) and DMPO (2 mM) were added to the samples, and the amount of DMPO-OH adduct was monitored by ESR measurements for 60 min. The zero time point was the H_2O_2 addition time, as described in Experimental Procedures.

(5.4) Time-Dependent Modulation of OH Radical Formation by Aggregated Aβ_{40}. We then monitored the time-dependent antioxidant activity of aggregated Aβ_{40}−Cu (I/II) complexes as compared to control (no Aβ_{40}) (Figures 9 and 10).

In the aggregated Aβ_{40}−Cu(II) complex, there is production of DMPO-OH adduct over time, and radical production is enhanced as compared to the control (Figure 9). Thus, in a 1 μM Aβ_{40} aggregate suspension, radical production was enhanced 5-fold, yet in a 20 μM Aβ_{40} aggregate suspension, the level of radical production was relatively reduced, as expected from the concentration-dependent activity of Aβ_{40} (Figure 7).

The aggregated Aβ_{40}−Cu(I) (homogeneous Aβ_{40} aggregate suspension) complex reduced the level of OH radical formation as compared to the control system during the first 20 min (Figure 10), similar to 10 μM soluble Aβ_{40} (Figure 3A).

DISCUSSION

The motivation for this study originated from the need to solve the current confusion regarding the anti- or pro-oxidant nature of Aβ_{40}, suggested on the basis of contradicting evidence (*12*,*63*−*65*). Understanding the role of the endogenous Aβ_{40} under normal physiological conditions and under oxidative stress is greatly important for the identification of potential therapeutic targets and, consequently, for the development of drug candidates, or therapeutic approaches.

Therefore, here, we targeted the study of the modulatory role of Aβ at the molecular level. We decided to avoid the complexity of living cells and to focus on Aβ_{40} in the simplest possible cell-free oxidative systems. For this purpose, we focused on the Cu(I)/Fe(II)-H_2O_2 oxidative systems. These low-valency metal ions represent the redox-reactive forms of Cu/Fe in Aβ_{40} responsible for catalyzing decomposition of H_2O_2 to $^{\bullet}OH$ (and ^{-}OH). In addition, we evaluated Aβ_{40} in the Cu(II)-H_2O_2 system as Cu(II) ions also induce OH radical production via H_2O_2 decomposition [although at a much lower rate than Cu(I)/Fe(II) ions] (*46*).

Our decision to evaluate the modulation of oxidative conditions by Aβ_{40} at the molecular level in cell-free systems to learn about oxidative stress in cells was justified by our finding that Aβ_{40} undergoes extensive oxidation at His6, His13, His14, and Tyr10 under cell-free conditions. This behavior is analogous to that of Aβ in senile plaques (*66*,*67*), leading us to conclude that our cell-free oxidative systems do indeed mimic AD oxidative stress conditions.

(1) Aβ_{40} Is a Remarkably Potent Antioxidant. We have found that Aβ_{40}, in either its soluble or its aggregated form, functioned as a remarkably potent antioxidant in metal ion-catalyzed radical-producing systems [Cu(I)/Fe(II)-H_2O_2]. We also found that Aβ_{40} functioned slightly less potently in the presence of Cu(II) (Table 1). Aβ_{40} proved to be 3.8−6.5-fold more potent than soluble Aβ_{28} in the Cu(I)/Fe(II)-H_2O_2 systems. Furthermore, it was 15−42 times more potent than Trolox, used as a standard in assays of total antioxidant capacity (*68*,*69*), in Cu(I)/Fe(II)-H_2O_2 systems (Table 1).

The presence of either soluble or aggregated Aβ_{40} in the Cu(I)-H_2O_2 system did not change the time-dependent inhibition pattern, as compared to the control system (Figures 3 and 10). However, for the Cu(II)-H_2O_2 system, a significant difference was observed between soluble and aggregated Aβ_{40} (Figures 4 and 9). For instance, 50 μM soluble Aβ_{40} slightly enhanced $^{\bullet}OH$ production with time, unlike the significant enhancement observed for the control system (Figure 4), yet 1 μM aggregated Aβ_{40} increased the level of $^{\bullet}OH$ formation as compared to the control system (Figure 9). Namely, time-dependent enhancement of ROS production will occur only if the following conditions prevail: low concentrations of aggregated Aβ_{40} in the presence of Cu(II).

(2) A Biphasic Modulation of Radical Formation Was Observed for Aβ_{40} in Cu(II)-H_2O_2 Systems. Soluble Aβ_{40} exhibited a biphasic modulation of radical formation in Cu(II)-H_2O_2 systems (Figure 2). We hypothesized that at low Aβ_{40} concentrations several Cu(II) ions bind to one Aβ_{40} molecule, resulting in an open coordination sphere of Cu(II). In this way, Cu(II) can bind a H_2O_2 molecule and electron transfer can occur. Since Aβ_{40} stabilizes Cu ions better than water (control), a pro-oxidant phase is obtained at low Aβ_{40} concentrations. At high Aβ_{40} concentrations, Aβ−Cu(II) complexes (e.g., 1:1 complexes) may involve a full Cu(II) coordination sphere. In this case, the H_2O_2 approach to the metal ion will be hindered, resulting in limited electron transfer and, eventually, inhibition of OH radical formation (an antioxidant phase).

The lack of a pro-oxidant phase at low Aβ_{40} concentrations, in the Cu(I)-H_2O_2 system, may be due to a greater stabilization of Cu(I) versus Cu(II) by Aβ_{40}. It was reported that when steric factors permit a tetrahedral arrangement of the ligands around a Cu(I) ion and at the same time prevent a square planar configuration around a Cu(II) ion, Cu(I) complexes will be favored over Cu(II) complexes (*70*).

If Aβ_{40} permits a tetrahedral arrangement, rather than a square planar one, of the ligands around a Cu(I) ion, it will result eventually in the lack of a pro-oxidant phase in the Cu(I) Fenton reaction.

At high Aβ_{40} concentrations where complexes of a different stoichiometry may form [e.g., 1:1 or 2:1 Aβ_{40}:Cu(I)], coordination with H_2O_2 is prevented. Subsequently, the Cu(I) Fenton reaction is inhibited.

(3) The Antioxidant Activity of Aβ_{40} Is Mainly Due to Radical Scavenging. Both Aβ_{28} and Aβ_{40} (either soluble or aggregated) were proposed to coordinate Cu(II) ions with three nitrogen atoms and one oxygen atom on the basis of EPR studies (*24*,*71*). Specifically, His residues (His6, His13, and His14) and an oxygen atom arising from either Asp1 (side chain carboxylate) (*57*) or Tyr10 (*7*) were suggested to be involved in Cu(II) coordination. Alternatively, two His residues and the amino-terminal nitrogen atoms were proposed to take part in the coordination (*72*). A 1:1 stochiometry was reported for the Cu(II)−Aβ_{40} complex (*73*,*74*).

Our findings here are indeed consistent with a 1:1 stochiometry. At ca. 0.12 mM Aβ_{40} and 0.1 mM Cu(II), a complete inhibition of H_2O_2 decomposition is observed, possibly implying the formation of a 1:1 Cu(II)−Aβ_{40} complex (Figure 2). Furthermore, our findings support the coordination of Cu and Fe ions to Aβ_{40} through His6, His13, His14, and Tyr10 (Table 2), as discussed below.

Aβ_{40} is a good Cu/Fe chelator (*73*,*75*,*76*). Therefore, Cu/Fe chelation by Aβ_{40} may contribute to the mechanism of inhibition of ROS formation. Aβ_{40} may provide the metal ions a full coordination sphere and a change in the redox potential (*8*,*24*,*76*−*78*), resulting in inhibition of electron transfer to H_2O_2. However, in addition to metal ion chelation, Aβ_{40} may inhibit OH radical production by scavenging OH radicals by its CH moieties.

We evaluated the contribution of the radical scavenging mechanism to the overall inhibition of OH radical production. For this purpose, we monitored the time-dependent oxidative damage to Aβ_{40} residues in the Cu(I/II)/Fe(II)-H_2O_2 systems by amino acid analysis. As OH radicals have an extremely short lifetime, their oxidative damage is expected to be most pronounced in the vicinity of the redox-active metal ion, where the radicals are formed. Hence, amino acids which coordinate the redox-active metal ion (His6, His13, His14, and Asp1 or Tyr10 residues) will be most susceptible to oxidative damage. Indeed, Aβ_{40} was practically completely oxidized after 24 h in Cu(I)/Fe(II)-H_2O_2 systems, whereas Aβ_{28} was only partially oxidized (Table 2). Therefore, we concluded that the primary (rapid) antioxidant activity of Aβ_{28} is mainly due to a metal ion chelation mechanism, while a secondary scavenging mechanism operates in a time-dependent manner (*36*).

Here, with IC_{50} values of Aβ_{40} which are up to 6.5-fold greater than those of Aβ_{28} in the same Cu(I)/Fe(II)-H_2O_2 systems, we certainly cannot consider metal ion chelation as the major mechanism. Specifically, metal ion coordination by Aβ occurs stoichiometrically (either 1:1 or 1:2 Aβ:metal ion) (*73*); therefore, the extremely low IC_{50} values of Aβ_{40} [e.g., 13 μM at 100 μM Fe(II)] cannot be explained on the basis of the metal ion chelation mechanism alone.

On the basis of this argument and the extensive oxidative damage caused to Aβ_{40} in Cu(I)/Fe(II)-H_2O_2 systems, even after 4 min, we propose that the major mechanism of antioxidant activity of Aβ_{40} is radical scavenging.

(4) Aβ_{40} Is a More Potent Antioxidant Than Aβ_{28} in Cu(I)/Fe(II)-H_2O_2 but Not Cu(II)-H_2O_2 Systems. IC_{50} values of both Aβ_{40} and Aβ_{28} in the Cu(II)-H_2O_2 system are identical (Table 1). Likewise, the His loss percentage in both Aβ_{28} and Aβ_{40} in the presence of Cu(II) ions (after either 21 min or 24 h) is practically the same. The identical behavior of Aβ_{28} and Aβ_{40} in this system is consistent with a similar affinity of Cu(II) for both Aβ_{28} and Aβ_{40} (*73*). Specifically, Simon et al. recently suggested that the peptide chain length has no influence on the metal ion binding constant value (log K_{app} is 9.4 for both Aβ_{40} and Aβ_{16}) (*73*).

Unlike the Cu(II)-H_2O_2 system, the Cu(I)/Fe(II)-H_2O_2 systems exhibit a significant difference between Aβ_{40} and Aβ_{28}. The antioxidant activity of Aβ_{40} is markedly enhanced compared to that of Aβ_{28} (Table 1). In addition, Aβ_{40} was substantially more oxidized than Aβ_{28} under these conditions (Table 2). These observations imply that the contribution of the radical scavenging component to OH radical inhibition is much more significant in Aβ_{40} than in Aβ_{28}.

We speculate that the significantly higher oxidative His loss in Aβ_{40} as compared to Aβ_{28} in the Cu(I)/Fe(II) systems reflects a different geometry and stability of the corresponding Aβ−Cu(I)/Fe(II) complexes.

The origin of this difference may be related to the nature of the coordinating Cu(II) and Cu(I) ions. Unlike Cu(II), Cu(I) and Fe(II) are soft ions and prefer coordination with soft ligands, e.g., sulfur atoms. We suggest that Cu(I) and Fe(II) coordinate with Aβ_{40} via the sulfur atom of Met35 in addition to His6, His13, His14, and Tyr10 (Scheme 1). As Met35 is not present in Aβ_{28}, Aβ_{28} is predicted to bind Cu(I) and Fe(II) with a lower affinity

than Aβ_{40}. This might explain the lower level of oxidative damage in Aβ_{28}.

Furthermore, binding of Cu(I)/Fe(II) via Met35 might explain the oxidative loss of Phe4, Lys16, Gln15, and Glu11 in Aβ_{40} (Table 2 and Scheme 1) due to the proximity of those amino acid residues to the redox center. This proximity is imposed by the tentative coordination of Met35 to Cu/Fe. As these structural changes do not occur in Aβ_{28}, Phe4, Lys16, Gln15, and Glu11 residues in the Aβ_{28}−Cu/Fe complex are not oxidatively lost.

Indeed, Raman data for the Aβ−Cu(II) complex within isolated plaque cores provide evidence of extensive Met35 oxidation (*79*). This evidence strongly supports the coordination of Met35 to Cu(I) [Fe(II)] ions.

The modulation of Cu/Fe-induced OH radical production by Aβ_{28} resulted in a sigmoidal decay of the OH radical concentration (*36*), yet modulation by Aβ_{40} resulted in an exponential decay of the OH radical concentration (Figure 2). These different inhibition patterns possibly reflect the differently weighted contributions of radical scavenging and metal ion chelation mechanisms in Aβ_{28} and also Aβ_{40} modulation.

The weighted contribution of radical scavenging to OH radical inhibition is more significant for Aβ_{40} than Aβ_{28}. Therefore, the effect of a very low Aβ_{40} concentration (ca. 1 nM) is significant in radical inhibition and results in an exponential decay graph, yet for Aβ_{28}, the weighted contribution of metal ion chelation to OH radical inhibition is more significant than for Aβ_{40}. Therefore, a relatively higher concentration of Aβ_{28} (ca. 60 nM) is required to obtain any antioxidant effect, resulting in a sigmoidal decay graph.

CONCLUSIONS

Earlier reports proposed a "dual role" of Aβ_{40}, where sequestration of metal ions by the monomer is neuroprotective, while Aβ aggregates generate oxygen radicals and cause neuronal death (*53*,*75*,*80*−*83*). Other studies suggested that early soluble oligomers are actually the toxic species responsible for neurodegeneration and neuronal cell death (*84*,*85*).

Our findings here for Aβ_{40} are in agreement with those reports proposing a neuroprotective role for the "monomeric" (soluble) protein. However, our data for the Aβ_{40} aggregates, which were found here to be highly potent antioxidants as well, are not in accord with many studies in the literature. OH radical formation was significantly inhibited by aggregated Aβ_{40} in a concentration- and time-dependent manner. Namely, Aβ_{40}−metal ion aggregates considered before to be deleterious oxidants appear here to be highly potent antioxidants.

Another argument found in the literature describes the oxidant versus antioxidant character of Aβ_{40} as being concentration-dependent. Namely, at nanomolar concentrations, Aβ_{40} is an antioxidant, whereas at micromolar concentrations, the antioxidant activity is abolished (*86*). Here, we found that Aβ_{40} was an antioxidant at either nanomolar or micromolar concentrations in Cu(I)/Fe(II) systems. In the Cu(II)-H_2O_2 system, Aβ_{40} was also an antioxidant, although at higher concentrations ($\geq 30\ \mu$M).

In summary, Aβ_{40} either soluble or aggregated, at either nanomolar or micromolar concentrations, is a highly potent antioxidant in cell-free oxidative systems, acting mainly as a radical scavenger. As mentioned above, these cell-free oxidative systems are adequate simulations of AD oxidative stress conditions. Therefore, we propose that it is not the Aβ_{40}−Cu(I)/Fe(II) complex per se that is responsible for the oxidative damage in AD.

REFERENCES

1. Andreasen, N., and Zetterberg, H. (2008) Amyloid-related biomarkers for Alzheimer's disease. *Curr. Med. Chem. 15*, 766–771.
2. Crouch, P. J., Harding, S.-M. E., White, A. R., Camakaris, J., Bush, A. I., and Masters, C. L. (2008) Mechanisms of Aβ mediated neurodegeneration in Alzheimer's disease. *Int. J. Biochem. Cell Biol. 40*, 181–198.
3. Selkoe, D. J. (1991) The molecular pathology of Alzheimer's disease. *Neuron 6*, 487–498.
4. Atwood, C. S., Huang, X., Moir, R. D., Tanzi, R. E., and Bush, A. I. (1999) Role of free radicals and metal ions in the pathogenesis of Alzheimer's disease. *Met. Ions Biol. Syst. 36*, 309–364.
5. Lovell, M. A., Robertson, J. D., Teesdale, W. J., Campbell, J. L., and Markesbery, W. R. (1998) Copper, iron and zinc in Alzheimer's disease senile plaques. *J. Neurol. Sci. 158*, 47–52.
6. Atwood, C. S., Moir, R. D., Huang, X., Scarpa, R. C., Bacarra, N. M. E., Romano, D. M., Hartshorn, M. A., Tanzi, R. E., and Bush, A. I. (1998) Dramatic aggregation of Alzheimer Aβ by Cu(II) is induced by conditions representing physiological acidosis. *J. Biol. Chem. 273*, 12817–12826.
7. Curtain, C. C., Ali, F., Volitakis, I., Cherny, R. A., Norton, R. S., Beyreuther, K., Barrow, C. J., Masters, C. L., Bush, A. I., and Barnham, K. J. (2001) Alzheimer's disease amyloid-β binds copper and zinc to generate an allosterically ordered membrane-penetrating structure containing superoxide dismutase-like subunits. *J. Biol. Chem. 276*, 20466–20473.
8. Rottkamp, C. A., Raina, A. K., Zhu, X., Gaier, E., Bush, A. I., Atwood, C. S., Chevion, M., Perry, G., and Smith, M. A. (2001) Redox-active iron mediates amyloid-β toxicity. *Free Radical Biol. Med. 30*, 447–450.
9. Schubert, D., and Chevion, M. (1995) The role of iron in β amyloid toxicity. *Biochem. Biophys. Res. Commun. 216*, 702–707.
10. Barrow, C. J., Yasuda, A., Kenny, P. T. M., and Zagorski, M. G. (1992) Solution conformations and aggregational properties of synthetic amyloid β-peptides of Alzheimer's disease. Analysis of circular dichroism spectra. *J. Mol. Biol. 225*, 1075–1093.
11. Zagorski, M. G., and Barrow, C. J. (1992) NMR studies of amyloid β-peptides: Proton assignments, secondary structure, and mechanism of an α-helix $\rightarrow$ β-sheet conversion for a homologous, 28-residue, N-terminal fragment. *Biochemistry 31*, 5621–5631.
12. Bush, A. I. (2003) The metallobiology of Alzheimer's disease. *Trends Neurosci. 26*, 207–214.
13. Tomiyama, T., Shoji, A., Kataoka, K.-I., Suwa, Y., Asano, S., Kaneko, H., and Endo, N. (1996) Inhibition of amyloid β protein aggregation and neurotoxicity by Rifampicin. Its possible function as a hydroxyl radical scavenger. *J. Biol. Chem. 271*, 6839–6844.
14. Huang, X., Moir, R. D., Tanzi, R. E., Bush, A. I., and Rogers, J. T. (2004) Redox-active metals, oxidative stress, and Alzheimer's disease pathology. *Ann. N.Y. Acad. Sci. 1012*, 153–163.
15. Fenton, H. J. H. (1894) Oxidation of tartaric acid in presence of iron. *J. Chem. Soc. 65*, 899–910.
16. Halliwell, B., Gutteridge, J. M. C., and Aruoma, O. I. (1987) The deoxyribose method: A simple "test-tube" assay for determination of rate constants for reactions of hydroxyl radicals. *Anal. Biochem. 165*, 215–219.
17. Burkitt, M. J., Tsang, S. Y., Tam, S. C., and Bremner, I. (1995) Generation of 5,5-dimethyl-1-pyrroline N-oxide hydroxyl and scavenger radical adducts from copper/H_2O_2 mixtures: Effects of metal ion chelation and the search for high-valent metal-oxygen intermediates. *Arch. Biochem. Biophys. 323*, 63–70.
18. Haber, F., and Weiss, J. (1934) The catalytic decomposition of hydrogen peroxide by iron salts. *Proc. R. Soc. London A147*, 332–351.
19. Weiss, J. (1935) Electron transition processes in the mechanism of oxidation and reduction reactions in solutions. *Naturwissenschaften 23*, 64–69.
20. Barb, W. G., Baxendale, J. H., George, P., and Hargrave, K. R. (1951) Reactions of ferrous and ferric ions with hydrogen peroxide. I. Ferrous-ion reaction. *Trans. Faraday Soc. 47*, 462–500.

21. Pecci, L., Montefoschi, G., and Cavallini, D. (1997) Some new details of the copper-hydrogen peroxide interaction. *Biochem. Biophys. Res. Commun. 235*, 264–267.
22. Gutteridge, J. M. C., and Wilkins, S. (1983) Copper salt-dependent hydroxyl radical formation. Damage to proteins acting as antioxidants. *Biochim. Biophys. Acta 759*, 38–41.
23. Huang, X., Atwood, C. S., Hartshorn, M. A., Multhaup, G., Goldstein, L. E., Scarpa, R. C., Cuajungco, M. P., Gray, D. N., Lim, J., Moir, R. D., Tanzi, R. E., and Bush, A. I. (1999) The Aβ peptide of Alzheimer's disease directly produces hydrogen peroxide through metal ion reduction. *Biochemistry 38*, 7609–7616.
24. Huang, X., Cuajungco, M. P., Atwood, C. S., Hartshorn, M. A., Tyndall, J. D. A., Hanson, G. R., Stokes, K. C., Leopold, M., Multhaup, G., Goldstein, L. E., Scarpa, R. C., Saunders, A. J., Lim, J., Moir, R. D., Glahe, C., Bowden, E. F., Masters, C. L., Fairlie, D. P., Tanzi, R. E., and Bush, A. I. (1999) Cu(II) potentiation of Alzheimer Aβ neurotoxicity. Correlation with cell-free hydrogen peroxide production and metal reduction. *J. Biol. Chem. 274*, 37111–37116.
25. Opazo, C., Huang, X., Cherny, R. A., Moir, R. D., Roher, A. E., White, A. R., Cappai, R., Masters, C. L., Tanzi, R. E., Inestrosa, N. C., and Bush, A. I. (2002) Metalloenzyme-like activity of Alzheimer's disease β-amyloid. Cu-dependent catalytic conversion of dopamine, cholesterol, and biological reducing agents to neurotoxic H_2O_2. *J. Biol. Chem. 277*, 40302–40308.
26. Irie, K., Murakami, K., Masuda, Y., Morimoto, A., Ohigashi, H., Ohashi, R., Takegoshi, K., Nagao, M., Shimizu, T., and Shirasawa, T. (2005) Structure of β-amyloid fibrils and its relevance to their neurotoxicity: Implications for the pathogenesis of Alzheimer's disease. *J. Biosci. Bioeng. 99*, 437–447.
27. Bush, A. I., Masters, C. L., and Tanzi, R. E. (2003) Copper, β-amyloid, and Alzheimer's disease: Tapping a sensitive connection. *Proc. Natl. Acad. Sci. U.S.A. 100*, 11193–11194.
28. Smith, M. A., Nunomura, A., Zhu, X., Takeda, A., and Perry, G. (2000) Metabolic, metallic, and mitotic sources of oxidative stress in Alzheimer disease. *Antioxid. Redox Signaling 2*, 413–420.
29. Smith, M. A., Joseph, J. A., and Perry, G. (2000) Arson. Track ing the culprit in Alzheimer's disease. *Ann. N.Y. Acad. Sci. 924*, 35–38.
30. Shigenaga, M. K., Hagen, T. M., and Ames, B. N. (1994) Oxidative damage and mitochondrial decay in aging. *Proc. Natl. Acad. Sci. U. S.A. 91*, 10771–10778.
31. Atwood, C. S., Obrenovich, M. E., Liu, T., Chan, H., Perry, G., Smith, M. A., and Martins, R. N. (2003) Amyloid-β: A chameleon walking in two worlds: A review of the trophic and toxic properties of amyloid-β. *Brain Res. Rev. 43*, 1–16.
32. Bush, A. I. (2000) Metals and neuroscience. *Curr. Opin. Chem. Biol. 4*, 184–191.
33. Varadarajan, S., Yatin, S., Aksenova, M., and Butterfield, D. A. (2000) Review: Alzheimer's amyloid β-peptide-associated free radical oxidative stress and neurotoxicity. *J. Struct. Biol. 130*, 184–208.
34. Markesbery, W. R. (1997) Oxidative stress hypothesis in Alzheimer's disease. *Free Radical Biol. Med. 23*, 134–147.
35. Kontush, A., Donarski, N., and Beisiegel, U. (2001) Resistance of human cerebrospinal fluid to in vitro oxidation is directly related to its amyloid-β content. *Free Radical Res. 35*, 507–517.
36. Baruch-Suchodolsky, R., and Fischer, B. (2008) Soluble amyloid β1−28-copper(I)/copper(II)/iron(II) complexes are potent antioxidants in cell-free systems. *Biochemistry 47*, 7796–7806.
37. Brenner, A. J., and Harris, E. D. (1995) A quantitative test for copper using bicinchoninic acid. *Anal. Biochem. 226*, 80–84.
38. Kalyanaraman, B. (1982) Detection of toxic free radicals in biology and medicine. *Rev. Biochem. Toxicol. 4*, 73–139.
39. Bitan, G., and Teplow, D. B. (2005) Preparation of aggregate-free, low molecular weight amyloid-β for assembly and toxicity assays. *Methods Mol. Biol. 299*, 3–9.
40. Ma, K., Clancy, E. L., Zhang, Y., Ray, D. G., Wollenberg, K., and Zagorski, M. G. (1999) Residue-specific pKa measurements of the β-peptide and mechanism of pH-induced amyloid formation. *J. Am. Chem. Soc. 121*, 8698–8706.
41. Esler, W. P., Stimson, E. R., Ghilardi, J. R., Lu, Y.-A., Felix, A. M., Vinters, H. V., Mantyh, P. W., Lee, J. P., and Maggio, J. E. (1996) Point substitution in the central hydrophobic cluster of a human β-amyloid congener disrupts peptide folding and abolishes plaque competence. *Biochemistry 35*, 13914–13921.
42. Hou, L., Shao, H., Zhang, Y., Li, H., Menon, N. K., Neuhaus, E. B., Brewer, J. M., Byeon, I.-J. L., Ray, D. G., Vitek, M. P., Iwashita, T., Makula, R. A., Przybyla, A. B., and Zagorski, M. G. (2004) Solution NMR studies of the Aβ(1−40) and Aβ(1−42) peptides establish that the Met35 oxidation state affects the mechanism of amyloid formation. *J. Am. Chem. Soc. 126*, 1992–2005.
43. Klug, G. M. J. A., Losic, D., Subasinghe, S. S., Aguilar, M.-I., Martin, L. L., and Small, D. H. (2003) β-Amyloid protein oligomers induced by metal ions and acid pH are distinct from those generated by slow spontaneous ageing at neutral pH. *Eur. J. Biochem. 270*, 4282–4293.
44. Mira, H., Vilar, M., Esteve, V., Martinell, M., Kogan, M. J., Giralt, E., Salom, D., Mingarro, I., Penarrubia, L., and Perez-Paya, E. (2004) Ionic self-complementarity induces amyloid-like fibril formation in an isolated domain of a plant copper metallochaperone protein. *BMC Struct. Biol. 4*, 7.
45. Klunk, W. E., Pettegrew, J. W., and Abraham, D. J. (1989) Quantitative evaluation of Congo red binding to amyloid-like proteins with a β-pleated sheet conformation. *J. Histochem. Cytochem. 37*, 1273–1281.
46. Baruch-Suchodolsky, R., and Fischer, B. (2008) Can nucleotides prevent Cu-induced oxidative damage?. *J. Inorg. Biochem. 102*, 862–881.
47. Ali, F. E., Separovic, F., Barrow, C. J., Yao, S., and Barnham, K. J. (2006) Copper and zinc mediated oligomerization of Aβ peptides. *Int. J. Pept. Res. Ther. 12*, 153–164.
48. Jao, S.-C., Ma, K., Talafous, J., Orlando, R., and Zagorski, M. G. (1997) Trifluoroacetic acid pretreatment reproducibly disaggregates the amyloid β-peptide. *Amyloid 4*, 240–252.
49. Shen, C.-L., and Murphy, R. M. (1995) Solvent effects on self-assembly of β-amyloid peptide. *Biophys. J. 69*, 640–651.
50. Szabo, Z., Klement, E., Jost, K., Zarandi, M., Soos, K., and Penke, B. (1999) An FT-IR study of the β-amyloid conformation: Standardization of aggregation grade. *Biochem. Biophys. Res. Commun. 265*, 297–300.
51. Barrow, C. J., and Zagorski, M. G. (1991) Solution structures of β peptide and its constituent fragments: Relation to amyloid deposition. *Science 253*, 179–182.
52. Li, L., Abe, Y., Kanagawa, K., Usui, N., Imai, K., Mashino, T., Mochizuki, M., and Miyata, N. (2004) Distinguishing the 5,5-dimethyl-1-pyrroline N-oxide (DMPO)-OH radical quenching effect from the hydroxyl radical scavenging effect in the ESR spin-trapping method. *Anal. Chim. Acta 512*, 121–124.
53. Hou, L., and Zagorski, M. G. (2006) NMR reveals anomalous copper(II) binding to the amyloid Aβ peptide of Alzheimer's disease. *J. Am. Chem. Soc. 128*, 9260–9261.
54. Walker, J. M. (2002) Nondenaturing polyacrylamide gel electrophoresis of proteins. In *The Protein Protocols Handbook* (Walker, J. M., Ed.) 2nd ed., Chapter 10, pp 57−60, Humana Press, Totowa, NJ.
55. Hicks, M., and Gebicki, J. M. (1986) Rate constants for reaction of hydroxyl radicals with Tris, Tricine and Hepes buffers. *FEBS Lett. 199*, 92–94.
56. Gelvan, D., and Saltman, P. (1990) Different cellular targets for copper- and iron-catalyzed oxidation observed using a copper-compatible thiobarbituric acid assay. *Biochim. Biophys. Acta 1035*, 353–360.
57. Guilloreau, L., Damian, L., Coppel, Y., Mazarguil, H., Winterhalter, M., and Faller, P. (2006) Structural and thermodynamical properties of Cu(II) amyloid-β16/28 complexes associated with Alzheimer's disease. *J. Biol. Inorg. Chem. 11*, 1024–1038.
58. Lashuel, H. A., and Grillo-Bosch, D. (2005) In vitro preparation of prefibrillar intermediates of amyloid-β and α-Synuclein. *Methods Mol. Biol. 299*, 19–33.
59. Nilsson, M. R. (2004) Techniques to study amyloid fibril formation in vitro. *Methods 34*, 151–160.
60. Zou, J., Kajita, K., and Sugimoto, N. (2001) Cu^{2+} inhibits the aggregation of amyloid β-peptide (1−42) in vitro. *Angew. Chem., Int. Ed. 40*, 2274–2277.
61. Sipe, J. D., and Cohen, A. S. (2000) Review: History of the Amyloid Fibril. *J. Struct. Biol. 130*, 88–98.
62. Walsh, D. M., and Selkoe, D. J. (2007) Aβ oligomers: A decade of discovery. *J. Neurochem. 101*, 1172–1184.
63. Smith, D. G., Cappai, R., and Barnham, K. J. (2007) The redox chemistry of the Alzheimer's disease amyloid β peptide. *Biochim. Biophys. Acta 1768*, 1976–1990.
64. Kontush, A. (2001) Alzheimer's amyloid-β as a preventive antioxidant for brain lipoproteins. *Cell. Mol. Neurobiol. 21*, 299–315.
65. Lee, H.-G., Zhu, X., Castellani, R. J., Nunomura, A., Perry, G., and Smith, M. A. (2007) Amyloid-β in Alzheimer disease: The null versus the alternate hypotheses. *J. Pharmacol. Exp. Ther. 321*, 823–829.

66. Atwood, C. S., Huang, X., Khatri, A., Scarpa, R. C., Kim, Y.-S., Moir, R. D., Tanzi, R. E., Roher, A. E., and Bush, A. I. (2000) Copper catalyzed oxidation of Alzheimer Aβ. *Cell. Mol. Biol. 46*, 777–783.
67. Hensley, K., Maidt, M. L., Yu, Z., Sang, H., Markesbery, W. R., and Floyd, R. A. (1998) Electrochemical analysis of protein nitrotyrosine and dityrosine in the Alzheimer brain indicates region-specific accumulation. *J. Neurosci. 18*, 8126–8132.
68. Halliwell, B., and Gutteridge, J. M. C. (2007) Free Radicals in Biology and Medicine, pp 658−659, Japan Scientific Societies Press, Tokyo.
69. Thomas, M. J., and Bielski, B. H. J. (1989) Oxidation and reaction of trolox c, a tocopherol analog, in aqueous solution. A pulse-radiolysis study. *J. Am. Chem. Soc. 111*, 3315–3319.
70. Perrin, D. D., and Hawkins, C. J. (1965) Oxidation-reduction potentials of copper complex ions. *Proceedings of the Australian Conference on Electrochemistry*, 1st ed., pp 115−123, Sydney, Hobart, Australia.
71. Karr, J. W., and Szalai, V. A. (2008) Cu(II) binding to monomeric, oligomeric, and fibrillar forms of the Alzheimer's disease amyloid-β peptide. *Biochemistry 47*, 5006–5016.
72. Karr, J. W., Akintoye, H., Kaupp, L. J., and Szalai, V. A. (2005) N-Terminal deletions modify the Cu^{2+} binding site in amyloid-β. *Biochemistry 44*, 5478–5487.
73. Hatcher, L. Q., Hong, L., Bush, W. D., Carducci, T., and Simon, J. D. (2008) Quantification of the binding constant of copper(II) to the amyloid-β peptide. *J. Phys. Chem. B 112*, 8160–8164.
74. Hong, L., Bush, W. D., Hatcher, L. Q., and Simon, J. (2008) Determining thermodynamic parameters from isothermal calorimetric isotherms of the binding of macromolecules to metal cations originally chelated by a weak ligand. *J. Phys. Chem. B 112*, 604–611.
75. Garzon-Rodriguez, W., Yatsimirsky, A. K., and Glabe, C. G. (1999) Binding of Zn(II), Cu(II), and Fe(II) ions to Alzheimer's Aβ peptide studied by fluorescence. *Bioorg. Med. Chem. Lett. 9*, 2243–2248.
76. Miura, T., Suzuki, K., and Takeuchi, H. (2001) Binding of iron(III) to the single tyrosine residue of amyloid β-peptide probed by Raman spectroscopy. *J. Mol. Struct. 598*, 79–84.
77. Jiang, D., Men, L., Wang, J., Zhang, Y., Chickenyen, S., Wang, Y., and Zhou, F. (2007) Redox reactions of copper complexes formed with different β-amyloid peptides and their neuropathalogical relevance. *Biochemistry 46*, 9270–9282.
78. Rottkamp, C. A., Atwood, C. S., Joseph, J. A., Nunomura, A., Perry, G., and Smith, M. A. (2002) The state versus amyloid-β: The trial of the most wanted criminal in Alzheimer disease. *Peptides 23*, 1333–1341.
79. Dong, J., Atwood, C. S., Anderson, V. E., Siedlak, S. L., Smith, M. A., Perry, G., and Carey, P. R. (2003) Metal binding and oxidation of amyloid-β within isolated senile plaque cores: Raman microscopic evidence. *Biochemistry 42*, 2768–2773.
80. Zou, K., Gong, J.-S., Yanagisawa, K., and Michikawa, M. (2002) A novel function of monomeric amyloid β-protein serving as an antioxidant molecule against metal-induced oxidative damage. *J. Neurosci. 22*, 4833–4841.
81. Khan, A., Dobson, J. P., and Exley, C. (2006) Redox cycling of iron by Aβ_{42}. *Free Radical Biol. Med. 40*, 557–569.
82. Monji, A., Utsumi, H., Ueda, T., Imoto, T., Yoshida, I., Hashioka, S., Tashiro, K.-I., and Tashiro, N. (2001) The relationship between the aggregational state of the amyloid-β peptides and free radical generation by the peptides. *J. Neurochem. 77*, 1425–1432.
83. Yang, E. Y., Guo-Ross, S. X., and Bondy, S. C. (1999) The stabilization of ferrous iron by a toxic β-amyloid fragment and by an aluminum salt. *Brain Res. 839*, 221–226.
84. Wang, H.-W., Pasternak, J. F., Kuo, H., Ristic, H., Lambert, M. P., Chromy, B., Viola, K. L., Klein, W. L., Stine, W. B., Krafft, G. A., and Trommer, B. L. (2002) Soluble oligomers of β amyloid (1−42) inhibit long-term potentiation but not long-term depression in rat dentate gyrus. *Brain Res. 924*, 133–140.
85. Walsh, D. M., Klyubin, I., Fadeeva, J. V., Cullen, W. K., Anwyl, R., Wolfe, M. S., Rowan, M. J., and Selkoe, D. J. (2002) Naturally secreted oligomers of amyloid β protein potently inhibit hippocampal long-term potentiation in vivo. *Nature 416*, 535–539.
86. Kontush, A., Berndt, C., Weber, W., Akopyan, V., Arlt, S., Schippling, S., and Beisiegel, U. (2001) Amyloid-β is an antioxidant for lipoproteins in cerebrospinal fluid and plasma. *Free Radical Biol. Med. 30*, 119–128.
87. Richter, Y., and Fischer, B. (2006) Nucleotides and inorganic phosphates as potential antioxidants. *J. Biol. Inorg. Chem. 11*, 1063–1074.